Ph. D. dissertation

Estimation of Time-Varying Sparse Underwater Acoustic Communication Channel Parameters

시변 스파스 수중 음향 통신 채널 매개변수 추정

Sung-Hoon Byun

August 2012

Department of Naval Architecture and Ocean Engineering

Seoul National University

Estimation of Time-Varying Sparse Underwater Acoustic Communication Channel Parameters

지도 교수 성 우 제

이 논문을 공학박사 학위논문으로 제출함
2012 년 8 월

서울대학교 대학원
조선해양공학과
변 성 훈

변성훈의 공학박사 학위논문을 인준함
2012 년 7 월

위 원 장 _____ (인)

부위원장 _____ (인)

위 원 _____ (인)

위 원 _____ (인)

위 원 _____ (인)

Abstract

This dissertation addresses the problem of estimating the channel parameters of time-varying sparse underwater acoustic communication channels. A new method to estimate the channel parameters including arrival time delay, incidence angle, Doppler frequency, and complex amplitude of impinging wave components is presented.

The new method exploits the sparse structure of the wideband underwater acoustic communication channel and is based on the matching pursuit which iteratively identifies multipath components by projecting the target signal on the columns of dictionary which are hypothesized by the channel parameters. Because of the large dimension of the parameter space, the size of dictionary can be prohibitively large especially when the parameter range is oversampled for effective sparse approximation.

In order to prevent the dictionary from being too large, the parameter estimation is achieved in two stages which are the identification and the iterative estimation stages. In the identification stage, the initial parameter values are identified using a pre-computed dictionary of low coherence. In the next estimation stage, a coherent and redundant dictionary of the oversampled parameter range is constructed from the identified parameter values, and the channel parameters are estimated by projecting the residual signal onto the redundant dictionary. To reduce memory requirement and computational complexity caused by using the redundant dictionary, a space-alternating estimation scheme is introduced to separate the parameter search space. The space-alternating scheme limits the size of the redundant dictionary within practical extent and accordingly reduces the computational burden of the matrix-vector product required in the iteration.

The performance of the new method is evaluated via Monte Carlo simulation and real channel measurement data analysis.

The Monte Carlo simulation evaluates the resolution performance by resolving two paths of small parameter differences, and its result shows that the new method successfully

decomposes multipath components whose parameter differences are merely a subfraction of the resolution limit of the classical correlation-based method.

It is also applied to the experimental data obtained in the large scale water tank which is capable of making a surface gravity wave with designated wave parameter. The channel parameters under the time-varying regular surface wave condition is analytically derived from a simple reflection constraint, and the channel parameters by the new channel estimation method are compared with those analytic solution showing that the estimation results are consistent with theoretical expectation.

Finally, it is applied to the real channel data of shallow water which were acquired at various transmitter-receiver ranges. The performance of the estimated channel parameters is evaluated indirectly via comparison of the channel characteristic functions which are the delay-Doppler-spread function, the angle-Doppler-spread function, and the power delay and angle profiles. The comparison result shows that the estimated channel parameters coincide well with the channel characteristic functions obtained by the matched filter and accordingly proves that the presented method gives consistent estimation result for the estimation of real channel parameters.

Index terms: Channel estimation, array signal processing, matching pursuit, greedy algorithm, sparse estimation, time-varying multipath channel.

Student number: 2006-30180

Table of Contents

List of Tables

List of Figures

Chapter 1
Introduction

Most of wireless communication system used in underwater environment depends on the acoustic signaling which still remains as the only way to send information to a remote receiver through the water. Although the acoustic signal with proper frequency propagates over long ranges, dynamic nature of the sea water environment imposes various effects on the acoustic channel so that accurate understanding of the channel is very important to design a reliable acoustic communication system.

Understanding the channel necessitates a precise method to get exact channel parameter information from measurement data, and the extracted channel parameter information can be used to make a channel model which becomes a basis to the communication system design.

It is the main subject of this thesis to devise an accurate, sophisticated channel estimation method for analyzing time-varying frequency selective underwater acoustic communication channels.

1.1 Background

Underwater acoustic communication channel is a rapidly time-varying multipath channel which makes it difficult to estimate the channel impulse response accurately. Its severely limited bandwidth and randomized time-varying multipath effects pose many obstacles to accurate channel estimation. The multipath effect is formed by the interaction with the waveguide boundaries and the sound refraction which is induced by the inhomogeneity of the water column. Because both the sea surface and the medium inhomogeneity changes in time, the underwater acoustic communication channel has time-varying characteristics which need to be modeled for developing an advanced acoustic communication systems operated in sea water.

Given the sufficient information on the channel environment, the existing numerical

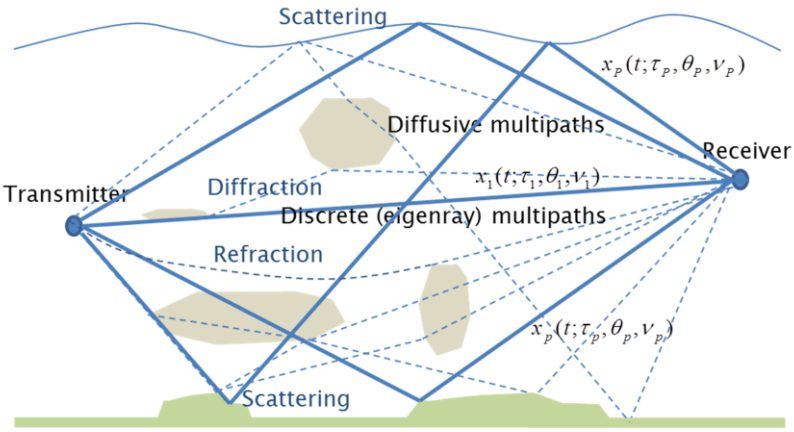

Fig. 1. Underwater acoustic communication channel and channel parameters.

propagation model matches quite well with the measured one at low frequencies [1]. However, the small scale fluctuation of the ocean makes the channel model at high frequencies deviate from the real channel impulse responses [2, 3]. The details of the fluctuation are known to vary considerably at different times and locations, which has impeded a unified channel model for evaluating the performance of the acoustic communication system. In order to fully understand the channel characteristics as well as the influence of the channel environmental conditions on them, a sophisticated channel estimation method is required to extract the channel parameters from the measured data thus enabling precise characterization of the statistics of channel parameters depicted in Fig. 1.

The large delay spread of the underwater acoustic channel implies that large number of channel taps has to be estimated and it in turn requires a long observation time window to afford such a large channel tap size. But rapid fluctuation and resulting short coherence time limit the length of the stationary signal samples so that the channel estimation becomes an ill-posed problem [4].

In order to overcome such difficulty, many recent researches focus on the sparse signal transmission structure which is prominent for the shallow water channel [3, 5-7]. In many shallow water environments, only a few echoes dominate the signal transmission, and accordingly a few taps of channel impulse response are responsible for representing a

received signal. Such sparsity can be exploited to give more stable solutions to the ill-posed channel estimation problem.

Before going into the main subject, we get a glimpse of the main problem treated in the thesis and give definitions of relevant terminology.

1.2 Definitions

A received signal at a receiver can be represented by superposition of multipath signals as expressed in

$$y(t) = \sum_{p=1}^{P} x_p(t;\Omega_p) + n(t) \tag{1.1}$$

where $x_p(t;\Omega_p)$ denote the pth multipath component, Ω_p is the channel parameter of the pth signal, and $n(t)$ is additive noise. Here, P denotes the number of multipath signals. Throughout this thesis, we use the baseband signal representation. Therefore $y(t)$, $x_p(t)$, and $n(t)$ are all complex values.

In particular, when the transmitted signal $s(t)$ undergoes time delay τ_p and Doppler shift ν_p, the received signal is expressed as

$$y(t) = \sum_{p=1}^{P} a(\Omega_p) e^{j2\pi\nu_p t} s\left(t - (\tau_p + a_p t)\right) + n(t) \tag{1.2}$$

where $\alpha(\Omega_p)$ denote the complex amplitude of the pth signal. Here, the Doppler shift ν_p and the compression or dilation factor a_p are related by

$$\nu_p = a_p f_c . \tag{1.3}$$

where f_c denotes the carrier frequency of the transmitted signal. In many cases, the signal model in (1.1) or (1.2) can be digitized and transformed into a canonical form of the linear inverse problem which is usually given by

$$\mathbf{y} = \mathbf{C}\mathbf{x} + \mathbf{n} \tag{1.4}$$

where $\mathbf{y}$ denotes the received signal vector, $\mathbf{x}$ is the unknown channel parameter vector, $\mathbf{C}$ is a known matrix usually determined by transmit signal, and $\mathbf{n}$ is the additive noise vector. $\mathbf{C}$ is referred to as a dictionary.

We say that the channel is sparse if the number of nonzero element of $\mathbf{x}$, which is denoted as P in (1.2), is significantly less than the dimension of $\mathbf{x}$, denoted by D. That is, only a few elements of channel parameter vector $\mathbf{x}$ have nonzero magnitude.

Thus the sparse channel parameter estimation problem is to solve (1.4) for $\mathbf{x}$ from a received signal vector $\mathbf{y}$ when P is significantly less than D.

1.3 Prior Work

Many previous attempts to estimate the channel parameters such as time delay and angle of impinging wave assumes the channel sparsity implicitly. For example, channel parameter estimation based on the maximum likelihood (ML) assumes that the number of signal sources is limited, and in many cases it is assumed that the number of sources is less than the number of quantized parameter range.

A noteworthy group of the ML approaches are those based on the Expectation-Maximization (EM) algorithm [8-12] which was originally presented in [13]. The EM algorithm for channel estimation first decomposes a received incomplete signal into multiple complete signals in the expectation (E) step and the parameters of each complete signal are estimated in the maximization (M) step [11]. The E step and M step are iterated to maximize the likelihood function until a prescribed halting rule is satisfied.

In [8, 9], the Space-Alternating Generalized Expectation-maximization (SAGE) algorithm was applied to channel parameter estimation problem. The SAGE algorithm was originally presented by [14] to introduce the space-alternating scheme for sequential update of parameters instead of simultaneous update of the original EM algorithm and is known to have improved convergence rate as well as lower computational complexity than the EM algorithm. Especially, [8-10] consider time-varying multipath channel parameter estimation and assume using a multichannel receiver array to estimate the incidence angle in addition to time delay, Doppler shift, and complex amplitude. It shares very similar problem formulation with this thesis. The SAGE algorithm is known to guarantee convergence to local maximum under suitable regularity condition but it requires good initial value to obtain the global maximum [14].

Whereas the EM and the SAGE algorithm do not explicitly talk about the sparsity of the channel, recent literature applies various sparse solutions such as the greedy algorithms and the optimization techniques to the sparse channel estimation problem.

The most well-known greedy algorithms are the matching pursuit (MP) [15] and its orthogonal variant, the orthogonal matching pursuit (OMP) [16]. They have been vigorously applied to the channel estimation problem [5, 17-21]. In particular, [17] uses the MP algorithm to estimate time-invariant multipath channel and compares it with the traditional LS method to show its simpler computation. However, it does not consider the time-variability of the channel and considers single element receiver case only. [5] deals with sparse time-varying underwater acoustic communication channel and adopts the delay-Doppler-spread function to parameterize the channel response both in delay and Doppler domain. In order to obtain a stable solution to the sparse problem, it uses the greedy algorithms such as the MP, the OMP and the order-recursive least square matching pursuit (LS-MP) to the real channel data. The data analysis results show that all the sparse processing methods have lower channel prediction error against the recursive least square (RLS) method with less computational complexity. Additionally, [5] considers time variability by including Doppler shift as the channel parameter and this results in better channel tracking capability when the channel

fluctuates rapidly. However, it assumes single element receiver and accordingly does not consider sparsity in angle domain. In [18, 19], the sparse channel tap detection problem was transformed into an equivalent on-off keying detection problem and an iterative detection and estimation scheme was proposed so that the location of zero taps were obtained by hard decision on initial channel estimate and then the non-zero tap gains were estimated in iterative manner. In [20], the MP and OMP were applied to the multicarrier underwater acoustic communication channel estimation and showed performance gain over the conventional frequency-domain channel estimation when tested with a field data collected in the shallow water. [21] also applies the channel sparsity to the multicarrier communication and obtains improved symbol estimation error performance with less complexity. The details of the MP and the OMP algorithms are discussed further in Section 2.2.

Whereas all of the sparse channel estimation introduced above are based on the greedy algorithm, [22-25] suggest that the optimization methods such as Dantzig selector and basis pursuit also can be used for reconstruction of the channel parameters. Their approaches are theoretically supported by the compressed sensing technique which guarantees the reconstruction performance when the dictionary satisfies the so-called restricted isometry property (RIP) condition [26]. However, those optimization methods are known to be computationally burdensome than the greedy algorithms [27].

We extend the sparse channel estimation suggested in [5] to include the incidence angle as the channel parameter to be estimated and use a new matching pursuit approach to estimate the channel parameters. In particular, the delay-Doppler-spread function defined in [5, 28] are extended to the angle-delay-Doppler-spread function. By utilizing a multichannel receiver array, an additional sparsity is gained in the incidence angle. Discriminating the incidence angle enhances multipath resolvability because the paths of the same time delay can be decomposed into different paths if their incidence angles are different. In addition, knowing the incidence angle of received signal reveals sound transmission structure which is important for channel modeling research which is one of the main themes of this thesis. Unlike the major of the previous studies which have focused on the channel estimation for equalization,

this study focuses on the accurate channel parameter estimation.

Although the sparse processing methods introduced in the literature give promising results, it should be noted that the sparse representation of the received signal is only effective when the signal parameters are exactly at the parameter discretization bins [29]. That is, if the Doppler shift or the incidence angle of the received signal is not exactly at the parameter discretization bins, the signal is represented by the superposition of multiple components with slightly different parameter values. In order to have fully sparse representation, the parameter range must be discretized with smaller intervals so that each of true parameter value can be matched to one of the discretized parameter candidates. But this causes the columns of the parameter-populated dictionary matrix to be redundant and coherent. Because of the increased parameter dimension, the oversampling of parameter range makes the size of dictionary become too large to be fitted into practical memory size and also requires heavy computation during the initial parameter identification for the MP and OMP method.

In this thesis, we present a new method to use the redundant dictionary for sparse channel parameter estimation. It adopts two-stage matching pursuit strategy where a pre-computed dictionary of low coherent columns, which is referred to as the global dictionary in this thesis, is used to identify the coarse parameter value, and then a redundant dictionary whose parameter ranges are densely sampled near the identified parameter value is used to estimate the precise parameter value. Such redundant dictionary is called as the local dictionary. The size of the redundant matrix is reduced further by parameter space alternating scheme. Thus the identification step globally searches the initial parameter value which best matches with the residual signal and then the iterative estimation step searches local optimum value near the identified one.

The basic assumption of the suggested method is that the channel has the sparse structure such that a few of quantized channel parameter range are responsible for most of the received signal energy. This is supported by many shallow underwater channel experiment data presented in [5, 18, 20, 24]. Another assumption is that the channel parameters, i.e., time delay, Doppler shift, incidence angle and complex amplitude, of each multipath component

are invariant during the observation time window and this is reasonable for short observation time of a few tens of milliseconds used in this study. Because it assumes a nonzero Doppler shift during the observation time, it has better channel variation tracking capability than the channel impulse response estimation which neglects Doppler shift.

1.4 Thesis Outline

The remainder of this dissertation is organized as follows:

Chapter 2 describes the underlying wideband multichannel signal model and derives the angle-delay-Doppler-spread function which is an extension of the delay-Doppler-spread function in [5, 28] to angular domain. It also discusses existing greedy algorithms and presents a new method called the space-alternating matching pursuit (SAMP).

Chapter 3 presents the performance evaluation via Monte Carlo simulation where the new method is applied to decompose two closely superimposed signals and estimates the parameters of each signal. The mean square error of the estimated parameters is analyzed to evaluate the resolution capability of the new method.

Chapter 4 deals with the experimental data analysis for verifying the consistency of the new method with real channel data which were obtained from the large scale water tank and the shallow sea water. For analysis of the water tank data, the surface reflected signal model is derived, and the channel parameter obtained from the data are compared with those by the derived reflection model. The performance of the new method is evaluated further using the shallow water experiment data which show sparse signal transmission structure. Because we do not know the true parameter values of the shallow water data, the consistency of the estimation results is evaluated indirectly using the channel characteristic functions.

Finally, in Chapter 5, concluding remarks are presented.

Chapter 2
Sparse Channel Estimation

In this chapter, we provide the time-varying multipath channel model assuming a multichannel receiver and transform it into a canonical formula which is appropriate for applying various solutions of linear inverse problem. The angle-delay-Doppler-spread function plays central role in the problem formulation.

Among the possible sparse solutions for the derived inverse problem, this thesis focuses on the greedy pursuit algorithm which is easy to implement and computationally practical. In order to achieve high resolution sparse channel parameter estimation, we use a redundant dictionary and propose a method to avoid practical issues caused by using the redundant dictionary.

2.1 Angle-delay-Doppler-spread Function

We assume that a wideband probe signal is transmitted through an underwater acoustic channel and a vertical linear receiver array with M sensors is used to observe the transmitted signal. If the compression or dilatation of the received signal is negligible, the received baseband signal at the *m*th sensor is expressed as

$$y_m(t) = \sum_p \alpha_p e^{j2\pi(m-1)\phi_p} e^{j2\pi\nu_p t} s\left(t - \left(\tau_p + \delta_{pm}\right)\right) + n_m(t), \qquad (2.1)$$

where $s(t)$ is the transmitted signal, $n_m(t)$ is additive ambient noise. τ_p, ν_p, α_p denote, respectively, the relative time delay, the Doppler shift and the complex amplitude of the *p*th multipath component and ϕ_p is its normalized angle which is defined by

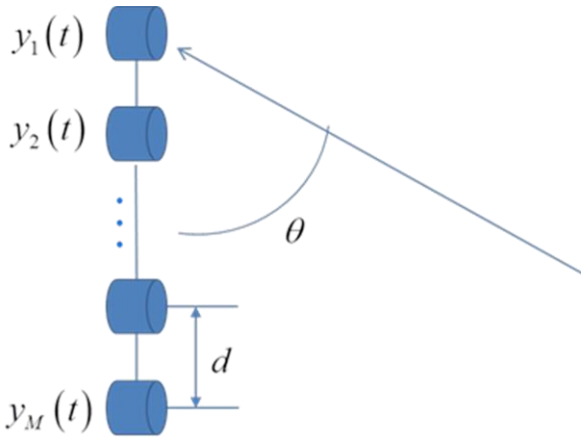

Fig. 2. Receiver array configuration.

$$\phi_p \triangleq \frac{d\cos\theta_p}{\lambda}. \tag{2.2}$$

Here, θ_p is the physical incidence angle (Fig. 2) and λ is the wavelength of the carrier wave. δ_{pm} in (2.1) denotes the array propagation delay at the *m*th sensor with respect to the array reference position which is designated as the first element position in this paper. Then, the array propagation delay is given by

$$\delta_{pm} = -\frac{(m-1)d\cos\theta_p}{c} = -\frac{(m-1)\lambda\phi_p}{c}. \tag{2.3}$$

In general, δ_{pm} is not negligible for wideband acoustic signaling where the ratio of the array size to the sound speed is comparable to the inverse of signal bandwidth but when the incidence angles of impinging waves are confined to be within small range from the array broadside as expressed in

$$\left|\frac{Md}{c}\cos\theta\right| \ll \frac{1}{B}, \tag{2.4}$$

δ_{pm} becomes very small and can be neglected.

If we discretize the parameter range and assume that the channel parameters in (2.1) belong to the discretized parameter set as

$\phi_p \in \{\phi_1, \phi_2, ..., \phi_j, ..., \phi_J\}$, where $\phi_j = \phi_1 + (j-1)\Delta\phi$,

$\tau_p \in \{\tau_1, \tau_2, ..., \tau_k, ..., \tau_K\}$, where $\tau_k = \tau_1 + (k-1)\Delta\tau$,

$\nu_p \in \{\nu_1, \nu_2, ..., \nu_l, ..., \nu_L\}$, where $\nu_l = \nu_1 + (l-1)\Delta\nu$,

the received signal in (2.1) can be approximated with the discretized channel parameters as follows:

$$y_m[i] = \sum_{j=1}^{J}\sum_{k=1}^{K}\sum_{l=1}^{L} \alpha_{j,k,l} e^{j2\pi(m-1)\phi_j} e^{j2\pi\nu_l i\Delta t} s_\delta(i\Delta t - \tau_k) + n_m[i] \qquad (2.5)$$

where $s_\delta(t) = s(t - \delta_{j,k,m})$ is the probe signal which is shifted by the array propagation delay according to the *j*th incidence angle, the *k*th delay discretization bin and Δt is sample time interval. $\alpha_{j,k,l}$ is the complex amplitude of the corresponding multipath component and it is denoted as the angle-delay-Doppler-spread function. The angle-delay-Doppler-spread function is an extended version of the delay-Doppler-spread function suggested in [5, 28, 30] and its magnitude implies the energy of multipath components belonging to each parameter discretization bin. So if the channel is sparse, then the majority of the terms in (2.5) become zero.

If $\delta_{j,k,m}$ is negligible, i.e., when (2.4) is satisfied, $s_\delta(t)$ becomes $s(t)$ and simpler expression of (2.5) is possible as follows. If we denote $s(i\Delta t)$ by $s[i]$ and $\Delta\tau$ is assumed to be same as Δt, (2.5) becomes

$$y_m[i] = \sum_{j=1}^{J}\sum_{k=1}^{K}\sum_{l=1}^{L}\alpha_{j,k,l}e^{j2\pi(m-1)\phi_j}e^{j2\pi\nu_l i\Delta t}s[i-k+1]+n_m[i]. \quad (2.6)$$

If we define the multichannel input delay-spread function, $h_m[i,k]$, as the Fourier transform of the angle-delay-Doppler-spread function $\alpha_{j,k,l}$, then the $h_m[i,k]$ is expressed as

$$h_m[i,k] = \sum_{j=1}^{J}\sum_{l=1}^{L}\alpha_{j,k,l}\exp\left(j2\pi(m-1)\phi_j\right)\exp\left(j2\pi\nu_l i\Delta t\right). \quad (2.7)$$

Applying (2.7) to (2.6) yields the canonical input-output relationship of the time-varying channel at the *m*th channel which is expressed as

$$y_m[i] = \sum_{k=1}^{K}h_m[i,k]s[i-k+1]+n_m[i]. \quad (2.8)$$

The problem at hand is to estimate the channel parameters shown in (2.5) or (2.6) from the received multichannel data samples, $y_m[i]$. The length of the data samples is denoted by I during which the channel parameters are assumed invariant. The transmit signal $s[i]$ is assumed to be known a priori.

In order to clarify the problem, (2.6) is expressed in vector notation as

$$y_m[i] = \left(\boldsymbol{\phi}_m \otimes \mathbf{v}[i] \otimes \mathbf{s}[i]\right)^T \mathbf{x} + n_m[i] \quad (2.9)$$

where

$$\boldsymbol{\phi}_m \triangleq \left[\, e^{j2\pi(m-1)\phi_1} \quad e^{j2\pi(m-1)\phi_2} \quad \cdots \quad e^{j2\pi(m-1)\phi_J} \,\right]^T, \quad (2.10)$$

$$\mathbf{v}[i] \triangleq \left[\, e^{j2\pi\nu_1 i\Delta t} \quad e^{j2\pi\nu_2 i\Delta t} \quad \cdots \quad e^{j2\pi\nu_L i\Delta t} \,\right]^T, \quad (2.11)$$

$$\mathbf{s}[i] \triangleq \left[s[i] \quad s[i-1] \quad \cdots \quad s[i-K+1] \right]^T, \tag{2.12}$$

$$\mathbf{x} \triangleq \left[\alpha_{1,1,1} \quad \cdots \quad \alpha_{1,1,K} \quad \cdots \quad \alpha_{1,L,K} \quad \cdots \quad \alpha_{J,L,K} \right]^T, \tag{2.13}$$

and $\otimes$ denotes the Kronecker product.

Stacking I successive samples of the received signal yields

$$\mathbf{y}_m[i] = \mathbf{C}_m[i]\mathbf{x} + \mathbf{n}_m[i] \tag{2.14}$$

where $\mathbf{y}_m[i]$ and $\mathbf{n}_m[i]$ are $I \times 1$ signal and noise vectors, respectively and $\mathbf{C}_m[i]$ is an $I \times D$ matrix with $D = JKL$ which are explicitly given by

$$\mathbf{y}_m[i] = \left[y_m[i] \quad y_m[i-1] \quad \cdots \quad y_m[i-I+1] \right]^T, \tag{2.15}$$

$$\mathbf{n}_m[i] = \left[n_m[i] \quad n_m[i-1] \quad \cdots \quad n_m[i-I+1] \right]^T, \tag{2.16}$$

and

$$\mathbf{C}_m[i] \triangleq \left[\mathbf{c}_{m,1} \quad \mathbf{c}_{m,2} \quad \cdots \quad \mathbf{c}_{m,D} \right]. \tag{2.17}$$

Here, the columns of $\mathbf{C}_m[i]$, (i.e., $\mathbf{c}_{m,1}[i], \mathbf{c}_{m,2}[i], \ldots$), are the angle-Doppler populated transmit symbol vector. The *d*th column of $\mathbf{C}_m[i]$ is given by

$$\mathbf{c}_{m,d} = \begin{bmatrix} e^{j2\pi(m-1)\phi_j} e^{j2\pi\nu_l(i-0)\Delta t} s\left[i-(k-1)-0 \right] \\ e^{j2\pi(m-1)\phi_j} e^{j2\pi\nu_l(i-1)\Delta t} s\left[i-(k-1)-1 \right] \\ \vdots \\ e^{j2\pi(m-1)\phi_j} e^{j2\pi\nu_l(i-I+1)\Delta t} s\left[i-k-I+2 \right] \end{bmatrix}. \tag{2.18}$$

where

$$k = (d-1) \bmod (K) + 1$$

$$l = \{(d-k)/K\} \bmod (L) + 1$$

$$j = \left\{ \frac{d-(l-1)K-k}{LK} \right\} \bmod (J) + 1$$

Therefore, the received signal vector $\mathbf{y}_m[i]$ is represented by the linear combination of the angle-Doppler populated symbol vectors with additive ambient noise. If we stack all M sensor data into single received signal vector and define the $IM \times D$ dictionary, $\mathbf{C}$, as follows:

$$\mathbf{C} \triangleq \left[\mathbf{C}_1^T \mid \mathbf{C}_2^T \mid \cdots \mid \mathbf{C}_M^T \right]^T, \tag{2.19}$$

Equation (2.14) becomes

$$\begin{aligned} \mathbf{y} &= \left[\mathbf{y}_1^T \quad \mathbf{y}_2^T \quad \cdots \quad \mathbf{y}_M^T \right]^T \\ &= \left[\mathbf{C}_1^T \mid \mathbf{C}_2^T \mid \cdots \mid \mathbf{C}_M^T \right]^T \mathbf{x} + \mathbf{n} \\ &= \mathbf{C}\mathbf{x} + \mathbf{n} \end{aligned} \tag{2.20}$$

where $\mathbf{n} = \left[\mathbf{n}_1^T \quad \mathbf{n}_2^T \quad \cdots \quad \mathbf{n}_M^T \right]^T$ is the $IM \times 1$ multichannel ambient noise vector. The time index, i, was omitted for brevity.

As a consequence, the channel parameter estimation using a multichannel receiver array is recast to the canonical linear inverse problem of solving (2.20) for the unknown $\mathbf{x}$ with the received signal vector $\mathbf{y}$ and the known dictionary matrix $\mathbf{C}$. The objective is to seek for the best approximation of the target signal $\mathbf{y}$ using the columns of the matrix $\mathbf{C}$ resulting in the coefficients of the columns which is $\mathbf{x}$.

A typical approach to (2.20) is the LS method which seeks for the solution of

$$\min_{\mathbf{x}} \left\| \mathbf{C}\mathbf{x} - \mathbf{y} \right\|_2 . \qquad (2.21)$$

Assuming that $\mathbf{C}$ has full column rank, the LS solution to (2.21) is given by

$$\hat{\mathbf{x}} = \left(\mathbf{C}^H \mathbf{C} \right)^{-1} \mathbf{C}^H \mathbf{y} . \qquad (2.22)$$

However, the usual approach based on the LS method may not give satisfactory result because of the large dimension of the unknown vector $\mathbf{x}$ with few nonzero entries. The large dimension and the sparse structure of $\mathbf{x}$ makes (2.20) overparameterized so that the LS solution (2.22) becomes unstable. This means that a small perturbation by additive noise $\mathbf{n}$ leads to largely different solution vector.

Instead of the LS method, sparse solution with sparsity constraint on $\mathbf{x}$ has become an appropriate choice. It finds a solution with the constraint that only a few entries of $\mathbf{x}$ are nonzero. If we seek for a solution of (2.21) satisfying the sparsity constraint that the number of nonzero elements in $\mathbf{x}$ is less than or equal to P, our problem in (2.20) can be restated as [31]

$$\min_{\mathbf{x}} \left\| \mathbf{y} - \mathbf{C}\mathbf{x} \right\| \text{ subject to } \left\| \mathbf{x} \right\|_0 \le P \qquad (2.23)$$

where $\left\| \cdot \right\|_0$ denotes the number of nonzero elements of the argument and P is the assumed number of multipath components. This problem is called as sparse approximation where the target signal $\mathbf{y}$ is approximated by linear combination of selected columns of $\mathbf{C}$. Both theoretical and experimental analysis appeared in [5, 18, 19] shows that the sparse processing has significant advantage for the sparse channel estimation in comparison with the LS method. When tested with the channel estimate based decision feedback equalizer, the sparse channel estimation gave lower bit error rate (BER) compared with the LS or RLS based channel

estimation method.

However, successful channel estimation by the sparse processing does not necessarily mean successful recovery of channel parameter itself. Even when the channel impulse response is estimated with sufficient accuracy, there may be ambiguity in the parameter estimation due to low dimensionality of the dictionary. That is, even if a received signal is approximated by a combination of selected columns of dictionary with small residual error, the relevant channel parameter may not be unambiguously determined if the parameter ranges used for making the dictionary are not sampled densely enough. This effect stands out when the signaling or measurement condition limits the resolution of the parameter estimation. In particular, the sparse channel estimation usually is successful for the time delay estimation under a sufficient signal bandwidth condition which discloses the sparse structure in the time delay domain. However, it may not be effective for the Doppler shift and incidence angle estimation where the length of observation time window and physical array are usually limited by channel coherence time and practical difficulties of enlarging the array aperture size. Such limitation makes the channel parameter in the corresponding domain become less sparse. This fact can be inferred from the discrete Fourier transform (DFT) relation between the multichannel input delay-spread function and the angle-delay-Doppler-spread function which was described in (2.7). Short observation time window and limited array length result in reduced resolution in the their Fourier transform domains and thus degrade the sparsity of the estimated channel parameters [32, 33].

The spectral sampling inherent for the discrete Fourier transform also makes the received signal less sparse. That is, even if a signal is received through single path channel, the received signal is represented only by the superposition of multiple signal components of different parameter values if its channel parameters are not exactly at the discretization bin. The usual way to overcome such situation is to oversample the parameter range. But the oversampling of parameter ranges causes the columns of dictionary to become coherent which obstructs stable recovery of $\mathbf{x}$ in (2.20) [29]. It also makes the size of the matrix too large to be hold with a practical size of memory.

A new approach to avoid these issues will be presented in Section 2.3 before which we take a brief review on the greedy algorithms applied previously for the sparse underwater acoustic channel estimation.

2.2 Orthogonal Matching Pursuit

As presented in Section 2.1, the time-varying sparse channel estimation problem can be converted to an inverse problem of which the solution is assumed sparse, and the goal is to estimate the angle-delay-Doppler-spread function given a noisy received signal.

There are numerous literatures dealing with such sparse inverse problem but we consider only the greedy algorithm in this thesis. Greedy algorithm iteratively searches the entries of the dictionary which are best correlated with the received signal and produces a sparse approximation of the target signal using the selected column vectors. Greedy algorithms are easy to implement and are known to be less computationally burdensome but it usually lacks of the theoretical guarantee for optimality [27, 31, 34]. Here, the optimality means the algorithm can guarantee the same error bound as the best known optimization based method.

Recently, new greedy algorithms such as the compressive sampling matching pursuit (CoSaMP) which guarantee the optimal performance were presented. But such optimality is guaranteed only when the RIP condition is satisfied for dictionary [31] and therefore it cannot be assured when a coherent dictionary is used as is in our case. Despite lack of theoretical performance guarantee, application to some experimental data supports that the greedy algorithms such as the MP and OMP are effective for estimating the time-varying sparse channel characteristics [5, 18, 20].

The MP algorithm iteratively identifies a column which best matches with the residual signal at each iteration and obtains the coefficient of the identified column by 1D projection of the residual signal onto it. The OMP algorithm is same as the MP except that the OMP recomputes the identified coefficients using the LS minimization of the distance between the identified columns and the target signal at each step. Thus if the columns of dictionary are

TABLE I
MP AND OMP ALGORITHMS

Input. Received signal $\mathbf{y} \in C^N$, dictionary $\mathbf{C} \in C^{N \times D}$.

Output. S-sparse channel parameters, $\{\tau_s, \theta_s, \nu_s, \alpha_s\}$ where $i \in \{1, 2, ..., S\}$

1) Initialize. Set the residual $\mathbf{r}_0 = \mathbf{y}$ and Let $s = 1$.

2) Identify.

Find $\mathbf{u}_s = \arg\max_{\mathbf{c}_j} \left| \mathbf{c}_j^h \mathbf{r}_{s-1} \right|$.

3) Estimate

$\mathbf{U}_s = \mathbf{U}_{s-1} \cup \mathbf{u}_s$

$\mathbf{x}_s = \arg\min_x \left\| \mathbf{r}_{s-1} - \mathbf{U}_s \mathbf{x} \right\|$

7) Update

$\mathbf{r}_s = \mathbf{y} - \mathbf{U}_s \mathbf{x}_s$.

Identify τ_s, θ_s, ν_s from $\mathbf{u}_s$ and $\alpha_s = x_s$.

$s = s + 1$.

Repeat (2) – (7) until stopping criterion is satisfied.

8) Output

Return $\Omega = \left\{ \{\tau_1, \theta_1, \nu_1, \alpha_1\}, \{\tau_2, \theta_2, \nu_2, \alpha_2\}, ..., \{\tau_S, \theta_S, \nu_S, \alpha_S\} \right\}$

orthonormal, then the MP and the OMP are basically the same. So hereafter we consider only the OMP algorithm without loss of generality.

Table I gives the description of the OMP algorithm for solving (2.20). Iteration ends when it meets the specified stopping criterion and the stopping criterion is related with the model order, i.e., the number of dominant paths which was denoted as P in Section 2.1, which is usually not known a priori. The model order suggests a trade-off between the variance of channel estimate and the undermodeling error caused by smaller model order [5]. Increasing the model order reduces the undermodeling error if the increased model order is close to the true value. On the other hand, it can increase the noise contribution when the assumed model order is larger than the true value. Therefore, for optimal channel estimate, the model order also must be estimated from the measured data [35, 36]. However, it requires additional computation burden so the following stopping criteria are often used instead [5, 31].

- Stopping after a fixed number of iteration.
- Stopping when there is no significant multipath component. i.e., $\left\| \mathbf{C}^H \mathbf{r}_{k-1} \right\|_\infty \le \varepsilon$.

- Stopping when the residual error becomes smaller than the prescribed threshold. i.e., $\left\|\mathbf{r}_{k-1}-\mathbf{U}_k\mathbf{x}\right\| \le \varepsilon$.
- Stopping when the residual error reduction is negligible. i.e., $\left|\left\|\mathbf{r}_{k-2}-\mathbf{U}_{k-1}\mathbf{x}\right\|-\left\|\mathbf{r}_{k-1}-\mathbf{U}_k\mathbf{x}\right\|\right| \le \varepsilon$.

Here, $\|\cdot\|_\infty$ denotes the maximum element of the argument and ε is the prescribed small value.

As discussed in Section 2.1, even an exactly sparse signal cannot be represented sparsely in the angle-delay-Doppler-spread function because the DFT relation in (2.7) deteriorates the signal sparsity by the inherent resolution limit and the spectral sampling. This can be easily confirmed by the simple simulation of two path channel where the parameters of the first arrival are set to be exactly at the integer multiple of sample interval whereas those of the second arrival are not. In particular,

$\tau_1 = 0 \cdot \Delta\tau = 0$ (symbols),

$\theta_1 = \theta_0 + 5 \cdot \Delta\theta = 0.5\pi$ (radians),

$\nu_1 = \nu_0 + 0 \cdot \Delta\nu = 0$ (Hz),

and

$\tau_2 = (10.2) \cdot \Delta\tau = 10.2$,

$\theta_2 = \theta_0 + (4.8) \cdot \Delta\theta = 0.6\pi$,

$\nu_2 = \nu_0 + (1.64) \cdot \Delta\nu = 16.08$.

where $\Delta\tau$, $\Delta\theta$ and $\Delta\nu$ are discretization interval of time delay, incidence angle and Doppler shift, respectively. It is noticed that the parameters of the second path is not an

integer multiple of the discretization interval. Both paths have equal magnitude. The signal bandwidth and the carrier frequency are 10 kHz and 25 kHz, respectively. An eight element receiver array with one wavelength spacing is used so that the unambiguous angle range is [$\frac{\pi}{3}$ $\frac{2\pi}{3}$]. Ten paths ($P=10$) was assumed in the processing. Although the conventional LS method attains lower mean square error, it does not give physically meaningful result in the presence of noise. It is because that the LS method is unstable for the overparameterized problem.

However, the OMP gives stable result for the same problem. Fig. 3 shows the channel estimation result obtained using the OMP algorithm for the two path channel simulation. As expected, the first arrival component is represented with single component but the second arrival component is represented with multiple components derogating the sparsity. Because of the spectral leakage, the magnitude of the second path is merely about a half of the first arrival. It is noteworthy that the parameter spread over the time delay axis is not much as other parameters. In the simulation, the signal bandwidth was relatively larger than the observation time duration and the array size so that the spectral leakage was minimized in the time delay axis.

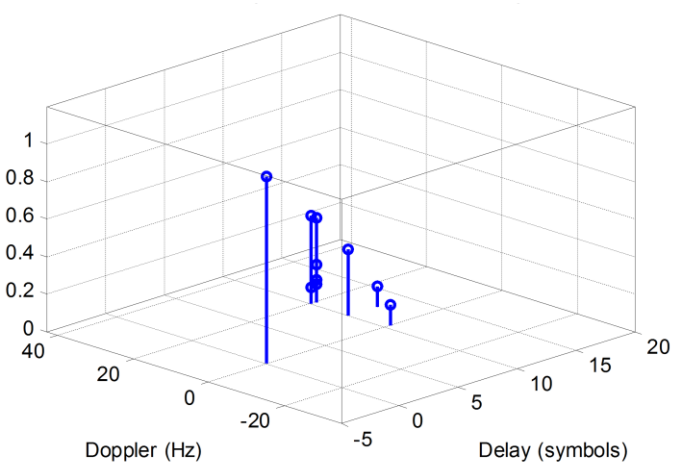

(a)

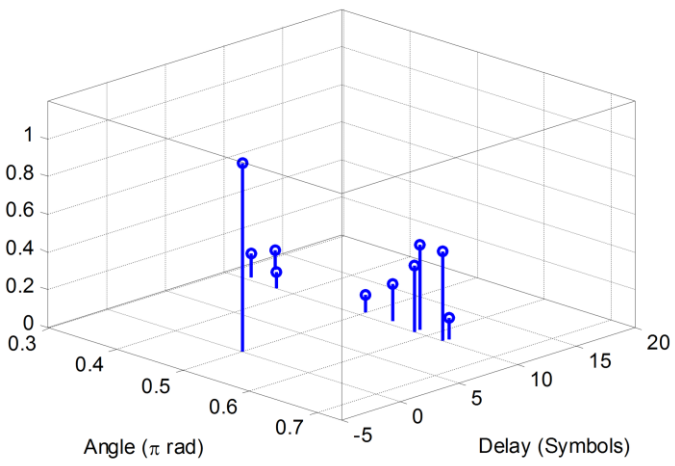

(b)

Fig. 3. Sparse estimation of the angle-delay-Doppler-spread function of the two path channel obtained by the OMP algorithm. The magnitudes of the estimated multipath components are shown in (a) Doppler-delay axis and (b) Angle-delay axis.

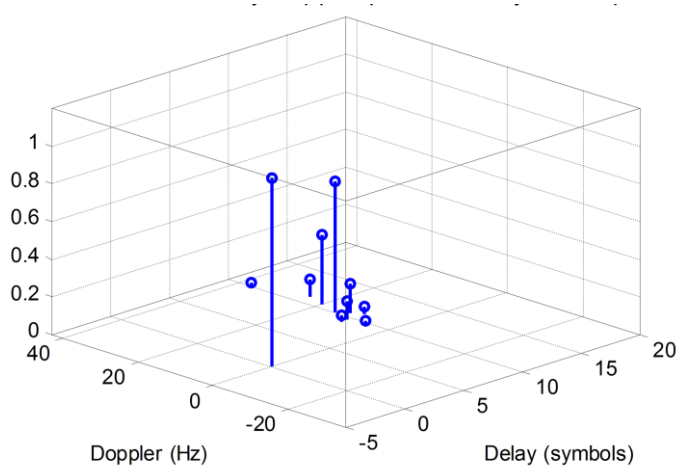

(a)

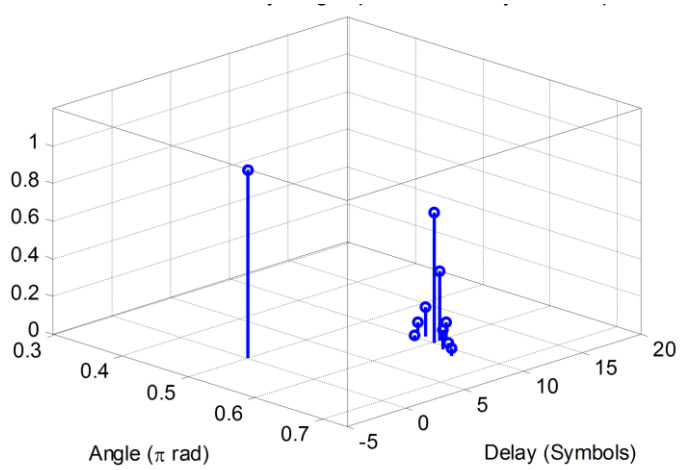

(b)

Fig. 4. Sparse estimation of the angle-delay-Doppler-spread function of the two path channel obtained by the OMP algorithm with oversampled parameter range. The magnitudes of the estimated multipath components are shown in (a) Doppler-delay axis and (b) Angle-delay axis.

As suggested earlier, a naïve way to reduce the sparsity degradation is to oversample the parameter range which is analogous to the oversampling of the Fourier transform domain in the DFT [29, 33]. To confirm the effect of parameter oversampling, we oversampled the parameter range such that the new parameter sample intervals, $\Delta\tau'$, $\Delta\theta'$ and $\Delta\nu'$, become

$$\Delta\tau' = \Delta\tau, \quad \Delta\theta' = \left(\frac{1}{2}\right)\cdot\Delta\theta, \text{ and } \quad \Delta\nu' = \left(\frac{1}{4}\right)\cdot\Delta\nu.$$

The channel estimation result for the oversampled parameter ranges is shown in Fig. 4. When compared with the result in Fig. 3, the spread over Doppler shift and incidence angle considerably has diminished, and the secondly largest magnitude has approached to the original magnitude. However, its magnitude is still smaller than that of the first path because of the spectral leakage.

Although the oversampling preserves the intrinsic channel sparsity, it makes dictionary too large. When the sample rate of each parameter is just doubled, the total column size of dictionary amounts to 2^3 times of the original matrix due to the dimension of the relevant parameter space. For the example given above, if the parameter ranges are sampled with J =16, K =40, and L =32, then the total column size of $\mathbf{C}$ amounts to 20480 and the total number of elements of the matrix becomes ~ 8e7 assuming that 510 time sample window and the eight element receiver array are used. Increased size of dictionary also imposes computational burden on the OMP algorithm which must identify the well-matched columns to the residual signal from the large dictionary. In general, the identification step of the OMP algorithm requires as many vector multiplication as the column size of the dictionary.

2.3 Space-Alternating Matching Pursuit

The OMP algorithm uses a fixed dictionary to approximate the target signal. Using a fixed dictionary for signal representation is justified by the sampling theorem which says any

signal of limited bandwidth can be represented in terms of the appropriate orthonormal basis such as the sinc function. But in the viewpoint of the channel parameter estimation, using only the orthonormal basis leads to insufficiently resolved parameter estimation and it necessitates a redundant linear vector space of oversampled parameters as discussed previously.

In order to constitute a redundant dictionary without enlarging its size, we employ an adaptive approach in which the reduction of dictionary size is accomplished via iteration of two-stage procedure: the identification stage and the estimation stage. In the identification stage, it searches coarse parameter value using a fixed and pre-computed global dictionary whose columns are produced by coarsely sampled parameter values such that the columns have low coherence. Here, the coherence μ is defined by

$$\mu = \max_{j \neq k} \frac{\left| \mathbf{c}_j^H \mathbf{c}_k \right|}{\left\| \mathbf{c}_j \right\| \left\| \mathbf{c}_k \right\|}. \qquad (2.24)$$

This means that the columns of the matrix have sufficient distance from each other so that the identification using 1D projection can determine stably which column is nearest to the residual signal vector. Instead of canceling out the identified column from the residual signal as the OMP does, it is merely provided as the initial guess to the subsequent estimation stage along with the parameter estimate.

In the estimation stage, a coherent dictionary for effective sparse approximation is constructed from the parameter value obtained in the identification stage. That is, the columns of the matrix are densely populated by the parameter values near the initial guess which were obtained from the previous stage. The presented algorithm is adaptive in the sense that the estimation stage is affected by the result of the previous identification stage. In order to reduce the dimension of the matrix further, the estimation stage is separated into multiple iterations alternating parameter space from which the name, space-alternating matching pursuit (SAMP), is derived. Table II describes the SAMP procedure.

TABLE II
SPACE-ALTERNATING MATCHING PURSUIT ALGORITHM

Input. Received signal $\mathbf{y} \in C^N$, dictionary $\mathbf{C} \in C^{N \times D}$

Output. S-sparse channel parameters, $\{\tau_i, \theta_i, \nu_i, \alpha_i\}$ where $\{\tau_i, \theta_i, \nu_i, \alpha_i\}$

1) Initialize.

Set the residual $\mathbf{r}_0 = \mathbf{y}$, and let $s = 1$

2) Identify.

Find $\mathbf{u}_{0,s} = \arg\max_{\mathbf{c}_j} \left| \mathbf{c}_j^h \mathbf{r}_{s-1} \right|$ and $\tau_{0,s}$, $\theta_{0,s}$, $\nu_{0,s}$ associated with $\mathbf{u}_{0,s}$. $\mathbf{c}_j$'s are columns of $\mathbf{C}$.

3) Estimate time delay.

Make local dictionary $\mathbf{C}_\tau \left(\Omega_\tau, \Omega_q, \Omega_\nu \right)$ with $\Omega_\tau = \left\{ \hat{\tau}_1, \hat{\tau}_2, ..., \hat{\tau}_{N_\tau} \right\}$, $\Omega_\theta = \left\{ \theta_{0,s} \right\}$, $\Omega_\nu = \left\{ \nu_{0,s} \right\}$.

Find $\mathbf{u}_{\tau,s} = \arg\max_{\mathbf{c}_{\tau,j}} \left| \mathbf{c}_{\tau,j}^h \mathbf{r}_{s-1} \right|$ and τ_s associated with $\mathbf{u}_{\tau,s}$. $\mathbf{c}_{\tau,j}$'s are columns of $\mathbf{C}_\tau$.

4) Estimate incidence angle.

Make local dictionary $\mathbf{C}_\theta \left(\Omega_\tau, \Omega_q, \Omega_\nu \right)$ with $\Omega_\tau = \left\{ \tau_s \right\}$, $\Omega_\theta = \left\{ \hat{\theta}_1, \hat{\theta}_2, ..., \hat{\theta}_{N_\theta} \right\}$, $\Omega_\nu = \left\{ \nu_{0,s} \right\}$.

Find $\mathbf{u}_{\theta,s} = \arg\max_{\mathbf{c}_{\theta,j}} \left| \mathbf{c}_{\theta,j}^h \mathbf{r}_{s-1} \right|$ and θ_s associated with $\mathbf{u}_{\theta,s}$. $\mathbf{c}_{\theta,j}$'s are columns of $\mathbf{C}_\theta$

5) Estimate Doppler shift.

Make local dictionary $\mathbf{C}_\nu \left(\Omega_\tau, \Omega_q, \Omega_\nu \right)$ with $\Omega_\tau = \left\{ \tau_s \right\}$, $\Omega_\theta = \left\{ \theta_s \right\}$, $\Omega_\nu = \left\{ \nu_1, \nu_2, ..., \nu_{N_\nu} \right\}$.

Find $\mathbf{u}_{\nu,s} = \arg\max_{\mathbf{c}_{\nu,j}} \left| \mathbf{c}_{\nu,j}^h \mathbf{r}_{s-1} \right|$ and ν_s associated with $\mathbf{u}_{\nu,s}$. $\mathbf{c}_{\nu,j}$'s are columns of $\mathbf{C}_\nu$

6) Merge

$\mathbf{u}_s = \mathbf{u}_{\nu,s}$,

$\mathbf{U}_s = \mathbf{U}_{s-1} \cup \mathbf{u}_s$,

$\mathbf{x}_s = \arg\min_x \left\| \mathbf{r}_{s-1} - \mathbf{U}_s \mathbf{x} \right\|$.

7) Update

$\mathbf{r}_s = \mathbf{y} - \mathbf{U}_s \mathbf{x}_s$,

$s = s + 1$.

Repeat (2) – (7) until stopping criterion is satisfied.

8) Output

$\alpha_s = x_s$, $s = 1, 2, ..., S$

Return $\Omega = \left\{ \left\{ \tau_1, \theta_1, \nu_1, \alpha_1 \right\}, \left\{ \tau_2, \theta_2, \nu_2, \alpha_2 \right\}, ..., \left\{ \tau_S, \theta_S, \nu_S, \alpha_S \right\} \right\}$

$\mathbf{C}_\tau$, $\mathbf{C}_\theta$ and $\mathbf{C}_\nu$ in Table II denote the coherent local dictionaries which are hypothesized by oversampled parameters. Previously estimated parameters are used in the subsequent parameter estimation so that τ_s is used to estimate θ_s and both are used to estimate ν_s . After the space-alternating iteration, the resulting symbol sequence vector $\mathbf{u}_s$ is merged with previously estimated linear space $\mathbf{U}_{s-1}$ to give updated linear subspace $\mathbf{U}_s$.

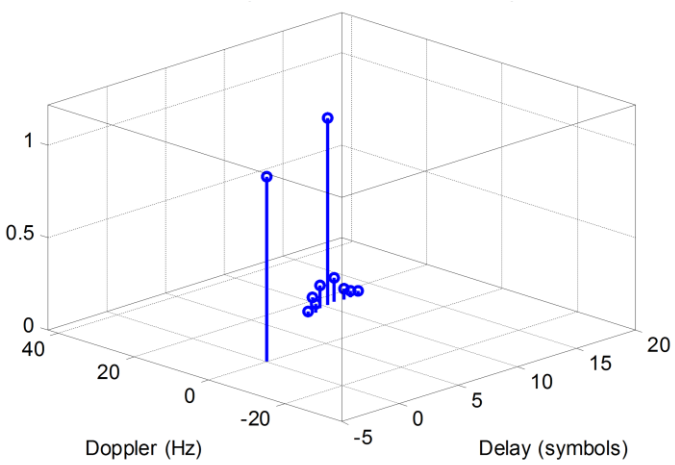

(a)

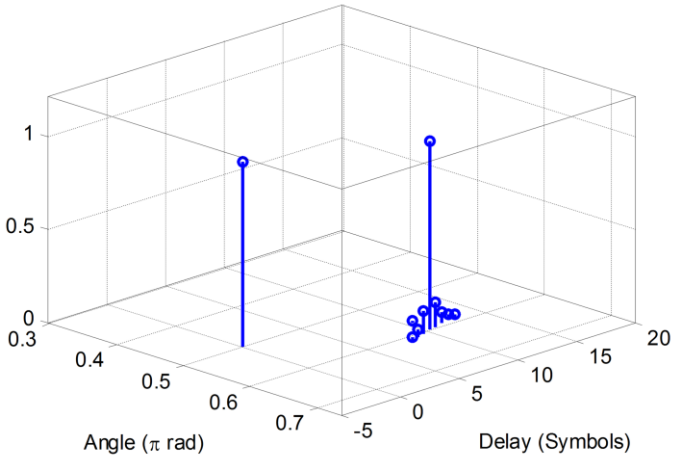

(b)

Fig. 5. Sparse estimation of the angle-delay-Doppler-spread function of the two path channel obtained by the SAMP algorithm. The magnitudes of the estimated multipath components are shown in (a) Doppler-delay axis and (b) Angle-delay axis.

Finally, the angle-delay-Doppler-spread function $\mathbf{x}_{s-1}$ is recomputed by the least square method resulting in $\mathbf{x}_s$ which minimizes the distance between the residual signal and the updated linear subspace represented by $\mathbf{U}_s$. By the estimation stage, the algorithm selects the most likely column from coherent local dictionary and subtracting it from the residual signal inhibits other coherent column from being selected in the subsequent iteration. Thus the

TABLE III
SUMMARY OF TWO PATH CHANNEL ESTIMATION RESULTS

	TRUE		OMP		OMP oversampled		SAMP	
	Path 1	Path 2	Path 1	Path 2	Path 1	Path 2	Path 1	Path 2
τ	0	10.2	0	10.0	0	10.0	0	10.0
θ	0.5π	0.6π	0.5π	0.625π	0.5π	0.603π	0.5π	0.599π
ν	0	16.08	0	19.608	0	14.706	0	16.238
$\lvert\alpha\rvert$	1	1	1	0.474	1	0.695	1	1.014

received signal is expressed in more sparse representation.

The new algorithm is applied to the previous two path channel simulation and its performance is compared with the OMP. In the processing of the step 3) to 5) in Table II,

N_τ = 40 samples per symbol period,

N_θ = 256 samples per unambiguous angle range $[\frac{\pi}{3}\ \frac{2\pi}{3}]$ (radians), and

N_ν = 256 samples per Doppler shift range [-39 39] (Hz)

are used. The columns of the matrices $\mathbf{C}_\tau$, $\mathbf{C}_\theta$ and $\mathbf{C}_\nu$ are generated by (2.5) and therefore it accounts for the array propagation delay. However, using (2.6) also gives indistinguishable result for the suggested case because the incidence angles are almost normal to the receiver array. Fig. 5 shows the channel parameters estimated by the new algorithm. The spectral leakage becomes negligible and thus the magnitudes of the two largest paths are almost same. Two path components are more clearly identified in comparison with the OMP results in Fig. 3 and Fig. 4. Parameter estimation errors are also smaller than the OMP results as summarized in Table III.

2.4 Computational Complexity

In this section, we discuss the computational complexity of previously introduced channel estimation methods including the SAMP method and suggest additional comments to reduce the complexity.

Before getting into the complexity of the SAMP, we first discuss the complexity of the LS method and the OMP. The conventional LS method uses the QR factorization to solve the linear inverse problem of (2.20) which usually takes the following steps [37],

Step 1. Compute QR factorization,

$$\mathbf{C} = \mathbf{QR} . \tag{2.25}$$

Step 2. Compute the vector,

$$\mathbf{Q}^{\mathbf{H}}\mathbf{y} . \tag{2.26}$$

Step 3. Solve the upper-triangular system,

$$\mathbf{Rx} = \mathbf{Q}^{\mathbf{H}}\mathbf{y} . \tag{2.27}$$

The most computationally intensive part of this conventional LS algorithm is the QR factorization step which is normally undertaken by Household triangularization. With the QR factorization, the complexity of the LS algorithm is given by [37]

$$O\left(2ND^2 - \frac{2}{3}D^3\right) \quad \text{flops.} \tag{2.28}$$

where N and D are the row and column sizes of the dictionary $\mathbf{C}$ defined in (2.20), and a flop means the operation counts required for multiplication of two floating point number and addition. Therefore if the row and column sizes are comparable to each other, the LS method requires $O\left(N^3\right)$.

The complexity of the OMP is mainly determined by the *Identify* and the *Estimate* step described in Table I. The *Identify* step finds a maximum inner product between the columns of the dictionary and the residual signal. It requires the matrix-vector multiplication which is accomplished by $O(ND)$ operations per iteration. The next *Estimate* step has to solve the LS problem but in this case the complexity can be reduced by maintaining a QR factorization over iterations. This is accomplished by performing the Gram-Schmidt orthogonalization [38]

at each iteration,

$$\mathbf{c}_{s+1}^{*}=\frac{\mathbf{c}_{s+1}-P_{V_s}\mathbf{c}_{s+1}}{\left\|\mathbf{c}_{s+1}-P_{V_s}\mathbf{c}_{s+1}\right\|}, \tag{2.29}$$

where $\mathbf{c}_{s+1}^{*}$ is the orthogonalized column, and P_s is a linear subspace spanned by

$$V_s=span\left\{\mathbf{c}_1^{*},\mathbf{c}_2^{*},...,\mathbf{c}_s^{*}\right\}. \tag{2.30}$$

In (2.29), P_{V_s} is the projection operation which is defined by

$$P_{V_s}\mathbf{c}_{s+1}=\sum_{i=1}^{s}\left\langle\mathbf{c}_{s+1},\mathbf{c}_i^{*}\right\rangle\mathbf{c}_i^{*}. \tag{2.31}$$

Calculation of (2.29) including (2.31) requires $O(Ns)\le O(ND)$ operations per iteration. If the number of paths is assumed S, the total amount of operations required for the *Identify* and the *Estimate* step marginally equals to $O(NDS)$. Comparing this with the complexity of the LS method which was given in (2.28), we can see that the complexity of the OMP is less than that of the LS method because the number of paths S is assumed far less than the total parameter size D in our problem .

Next, we analyze the complexity of the SAMP in Table II. The complexity of the SAMP is inevitably higher than that of the OMP because the initial step (1) and the last two steps (6-7) of the SAMP are actually equivalent to the OMP while the steps between them add significant extra complexity to the original OMP method. Such extra complexity can be divided into two parts: one is to make the local dictionary with respect to the identified parameter values and the other is to process the matching pursuit with the local dictionary. If we denote the operation count required for calculating a column of the local dictionary as

TABLE IV
RUNNING TIME OF CHANNEL ESTIMATION BY LS, OMP, AND SAMP

Method	LS	OMP	SAMP
Time (sec)	1.62	0.15	8.19

*MEASURED WITH MATLAB 64 BIT VERSION 7.12 ON INTEL CORE I7 1.6 GHZ.

$O(\ell)$, and denote the quantization size of a parameter β as D_β, the operation counts required for making a local dictionary simply amount to $O(\ell D_\beta)$. The subsequent matching pursuit processing also requires $O(ND_\beta)$ operations. It should be noted that $O(\ell)$ is by no means the first order polynomial operation count and ℓ was introduced just for notational convenience. The actual operation count of ℓ is dependent on the trigonometric function calculation as well as time shifting operation as described in the following formula used for making a column of the local dictionary,

$$c(\tau_k,\theta_k,\nu_k)=\begin{bmatrix} e^{j2\pi 0\phi_j}e^{j2\pi\nu_l 0\Delta t}s_\delta(0\Delta t-\tau_k) \\ e^{j2\pi 0\phi_j}e^{j2\pi\nu_l 1\Delta t}s_\delta(1\Delta t-\tau_k) \\ \vdots \\ e^{j2\pi(m-1)\phi_j}e^{j2\pi\nu_l i\Delta t}s_\delta(i\Delta t-\tau_k) \\ \vdots \\ e^{j2\pi(M-1)\phi_j}e^{j2\pi\nu_l(I-2)\Delta t}s_\delta((I-2)\Delta t-\tau_k) \\ e^{j2\pi(M-1)\phi_j}e^{j2\pi\nu_l(I-1)\Delta t}s_\delta((I-1)\Delta t-\tau_k) \end{bmatrix}. \qquad (2.32)$$

In order to get a practical sense of the discussed complexity, we measured the running time of the algorithms for the two path channel example suggested in the previous sections. The running time was measured for the core part of each algorithm implemented with Matlab, and the results are summarized in Table IV. As shown in the table, the running time of the LS is about $11\times$ of the OMP, and that of the SAMP is $55\times$ of the OMP. This means that the computational complexity of the SAMP is far higher than the OMP and even higher than the LS method.

This high complexity can be mitigated for the case when the propagation delay within

the array is negligible as expressed in (2.4). If we consider the time delay estimation, i.e., the third step in Table II, the signal at time index i can be approximately expressed by

$$y_m[i] \approx \sum_{k=1}^{K} \alpha_{j_0,k,l_0} e^{j2\pi(m-1)\hat{\phi}_{j_0}} e^{j2\pi\hat{\nu}_{l_0} i\Delta t} s[i-k+1] + \sum_{j\neq j_0}\sum_{l\neq l_0}\sum_{k} \alpha_k e^{j2\pi(m-1)\phi_j} e^{j2\pi\nu_l i\Delta t} s[i-k+1] + n_m[i] \tag{2.33}$$

where $\hat{\phi}_{j_0}$ and $\hat{\nu}_{l_0}$ are the initial guess of incidence angle and Doppler shift by the Identify step, and $n_m[i]$ is the additive noise at the *m*th sensor.

If we combine the multichannel data and compensate the Doppler shift using $\hat{\phi}_{j_0}$ and $\hat{\nu}_{l_0}$ as follows:

$$z[i] \triangleq \frac{1}{M}\sum_{m} e^{-j2\pi(m-1)\hat{\phi}_{j_0}} e^{-j2\pi\hat{\nu}_0 i\Delta t} y_m[i], \tag{2.34}$$

the resulting signal $z[i]$ can be expressed as

$$z[i] = \sum_{k=1}^{K} \alpha_k s[i-k+1] + R'_{s+1} + n'[i] \tag{2.35}$$

where R'_{s+1} is the residual interference signal and $n'[i]$ is the multichannel-combined additive noise. If we regard R'_{s+1} and $n'[i]$ as a noise term, solving for α_k from (2.35) becomes the conventional time-invariant channel estimation problem and the computationally efficient scheme can be exploited. Especially when the probe signal is periodic, the solution for (2.35) can be obtained using the fast Fourier transform (FFT) algorithm in the same way as the orthogonal frequency-division multiplexing (OFDM) channel estimation [20, 39]. In addition, under the negligible array propagation delay assumption, the multichannel

combining of (2.33) is equivalent to the narrowband beamforming which also can be implemented by the FFT algorithm [40, 41]. However, the FFT processing of (2.35) using the periodic channel probing signal implicitly requires that hypothesized time delay range is sampled at intervals of symbol period, and it results in poor resolution of the time delay estimation. In that case, a precise peak location algorithm such as the parabola fitting can be used [42].

Chapter 3
Parameter Estimation of Synthetic Channel

Performance evaluation of the presented estimator is also an important issue which must be handled properly. Theoretical performance bound analysis based on the Cramer-Rao bound (CRB) is possible for simple channel cases but it is not obtainable for most of the realistic channel conditions. So the performance evaluation often depends on the numerical simulation where the received signal is synthesized using predetermined channel conditions, and the parameter estimated from the signal are compared with the true ones used for signal synthesis. However, the underwater acoustic channel model used for signal synthesis are not exactly matched to the real channels and thus the performance statistic using the simulation data can deviate from the practical performance to the real channel data. Therefore application of the presented method to the experimental data is required to assure its applicability to real channels.

We evaluate the performance of the presented algorithm via numerical simulation, water tank experiment data analysis, and shallow sea water channel data analysis. The result of the numerical simulation is treated in this chapter and those of experimental data analysis will be given in the next chapter.

3.1 Performance Evaluation Method

Before discussing the performance evaluation results, it is worth summarizing here the performance evaluation methods taken in the prior works. The performance criteria used in the literature can be categorized into

- Cramer-Rao Bound (CRB) analysis [8, 19].
- Signal residual prediction error [5].
- BER performance of equalization based on the channel estimate [5, 18].

- Mean square error (MSE) analysis via Monte Carlo simulation [8, 18].
- Comparison of the reproduced signal with the measured signal [8].
- Identification of channel environment with the channel estimate [5, 8].

The CRB shows the theoretical performance bound of the unbiased estimator when the probabilistic density function (pdf) of noise satisfies certain regularity conditions such that the following Fisher information $I(\lambda)$ can be defined

$$I(\lambda) = E\left[\left(\frac{\partial f(x;\lambda)}{\partial \lambda}\right)^2\right] = -E\left[\frac{\partial^2 f(x;\lambda)}{\partial \lambda^2}\right] \tag{3.1}$$

where $f(x;\lambda)$ stands for the pdf of random variable (noise) x which is dependent on the parameter λ. In [8], the authors analyze the performance of their suggested method for two path channel using the CRB under Gaussian noise assumption and compares it with Monte Carlo simulation. By the comparison, they prove that their method attains the CRB when the channel parameters are separated with only small differences which are less than the resolution limit required by the classical correlation based method. This resolution limit of the classical method will be discussed in Section 3.2. [19] derives the CRB of time invariant sparse channel estimation under the assumption of perfect knowledge of zero tap location and proves that the sparse estimation gives smaller estimation error, i.e. lower CRB, than the conventional LS method. Although the CRB's discussed in the references provide a firm theoretical basis, achievability of such basis is rather conditional because the assumptions used for the CRB derivation cannot be generally satisfied by real channels.

The second and the third criteria are closely related to communication system perspective which is mainly interested in the compensation of channel distortion and error-free symbol recovery with low computational complexity. In [5], the accuracy of the channel estimation is evaluated by the signal residual prediction error which is defined by

$$\varepsilon[i+1] \triangleq \left| y[i+1] - \hat{y}[i+1|i] \right|^2 \qquad (3.2)$$

where $y[i+1]$ is the true signal and $\hat{y}[i+1|i]$ is the predicted signal based on the channel estimate at time i. The BER after channel equalization using the sparse channel estimation also can be used to evaluate the plausibility of the channel estimate [5, 18]. Such performance evaluation criteria are focused on the ability to approximate a target signal using low dimensional dictionary whose columns have low coherence and this in turn implies that coarsely sampled parameter-populated dictionary is used. So even if low BER or good signal prediction performance is achieved, poor resolution capability of coarsely sampled parameters raises an issue about the accuracy of the parameter itself as was discussed in Chapter 2.

The MSE analysis via Monte Carlo simulation evaluates the estimation performance and the stability of the presented algorithm to noisy synthesis data. It can show various aspects of estimation performance by controlling the simulation conditions and can be applied to fairly complex channel cases. However, the performance statistic with the synthesized data can deviate from that with real channels because the exact statistical properties of the underwater acoustic channel cannot be perfectly realized. To prove the convergence of the estimator for the real channels, the MSE analysis via numerical simulation is usually supplemented with some kind of real channel data analysis.

The last two criteria, which are the signal reproduction and the channel environment identification, are usually used for the experimental data analysis where the information of the true channel parameters is not available. The evaluation via the signal reproduction reconstructs a received signal from the estimated channel parameters using the known transmitted signal and compares it with the measured signal to evaluate the quality of the channel estimate [8]. It is based on the belief that large coherence between the reconstructed and the received signals means close resemblance of the channel parameter estimate to the unknown true parameters. The channel environmental identification seeks for the environmental features which can explain the estimated channel parameters. For example, in

[5], the signal prediction error were compared with the surface wave height log so that the error peaks were identified with the dynamic events induced by the surface wave motion. In [8], the estimated channel parameters are identified with reflectors or scatterers which are located around the experiment site so that the estimation performance are analyzed in qualitative manner. Although those indirect comparisons do not provide any exact measure of the estimation performance, they can support the proximity of the estimation results to the true parameter values which are not available for experimental data.

In this study, we evaluate the resolution performance of the SAMP by the Monte Carlo method and test its applicability to the real channel by analyzing experimental data obtained from a water tank and the shallow sea water.

3.2 Mean Square Error Performance

The resolution of the SAMP is evaluated by a Monte Carlo simulation. Similar to the example dealt with in the previous section, two-path channel is considered but their channel parameters are set to be very close at this time. The channel parameters are varied to analyze the variation of resolution performance according to the parameter difference. The magnitudes of two paths are set to be equal as before. The detailed information of the simulation condition is given in Table V. As shown in Table V, the parameter difference is merely a fraction of the resolution limit of the classical correlation or beamforming based method which are given by [8]

$$\tau_c = T_{sym}, \quad \theta_c = \frac{2}{M}, \text{ and } \quad \nu_c = \frac{1}{T_w} \tag{3.3}$$

where T_{sym} is symbol period and T_w is the observation time window both in seconds. Here, τ_c, θ_c, and ν_c are the time delay resolution limit by the cross correlation method, the angle resolution limit by the conventional beamforming method, and the Doppler shift resolution

TABLE V
SUMMARY OF TWO PATH CHANNEL MONTE CARLO SIMULATION

Parameter	Value
Carrier frequency (f_c)	25 kHz
Symbol rate ($f_{sym} = 1/T_{sym}$)	10 kHz
Pulse shaping filter	Root-raised-cosine filter (order = 20, rolloff factor = 0.35)
Number of array elements (M)	8
Array element spacing (d)	one wavelength (unambiguous angle = [$\frac{\pi}{3}$ $\frac{2\pi}{3}$])
Transmit signal	255 symbol PN sequence
Observation time window (T_w)	25.5 milliseconds (= $255 \times T_{sym}$)
Time delay interval (N_τ)	40 samples per one symbol period
Angle interval (N_θ)	128 samples per unambiguous angle range
Doppler shift interval (N_ν)	128 samples per Doppler shift range [-39 39] (Hz)
Time delay difference ($\Delta\tau$)	[0.2:0.2:1.2]$\cdot \tau_c$
Incidence angle difference ($\Delta\theta$)	[0.0:0.2:1.0]$\cdot \theta_c$
Doppler shift difference ($\Delta\nu$)	[0.0:0.2:1.0]$\cdot \nu_c$
Number of runs	100

limit by the periodogram-based spectrum estimation method, respectively. Spatially and temporarily white Gaussian noise is added to the signal such that the input signal-to-noise ratio equals 0 dB. The number of multipath components is assumed to be known. The parameters of two paths are set in the simulation as follows:

$$\tau_1 = 0, \quad \tau_2 = \Delta\tau \cdot \tau_c,$$

$$\theta_1 = 0.5\pi - \Delta\theta \cdot \theta_c, \quad \theta_2 = 0.5\pi + \Delta\theta \cdot \theta_c,$$

$$\nu_1 = 0, \text{ and } \quad \nu_2 = \Delta\nu \cdot \nu_c / 2$$

To assess the resolution performance of the new algorithm, the root-mean-square estimation error (RMSEE) of each parameter is analyzed. The RMSEE of a parameter β is defined by

$$\mathrm{RMSEE}(\beta)=\sqrt{\frac{1}{N}\sum_{n=1}^{N}\left(\hat{\beta}-\beta_{true}\right)^2}\,. \qquad (3.4)$$

where $\hat{\beta}$ and β_{true} denote the estimated parameter value and the true parameter value, respectively, and N is the number of simulation runs. Thus the low RMSEE means that the two paths were successfully separated and their parameter were accurately estimated.

The RMSEE's of the magnitude of the first path are shown in Fig. 6. Fig. 6(a) shows the RMSEE's of $\hat{\alpha}_1$ over different $\Delta\tau$ and $\Delta\theta$ when the Doppler shifts of two paths are zero. Fig. 6(b) shows the RMSEE's of $\hat{\alpha}_1$ over different $\Delta\theta$ and $\Delta\nu$ when $\Delta\tau$=0.2τ_c, and Fig. 6(c) is same as Fig. 6(b) except that $\Delta\tau=\tau_c$. Because of larger time delay difference, Fig. 6(c) shows lower RMSEE than Fig. 6(b). As expected, the RMSEE's decrease with increasing parameter differences, and they are below one tenth of the true value in all cases. This implies that the new method successfully resolved the two multipath components whose parameter differences are below the classical limits which is given in (3.3).

The RMSEE's of $\hat{\alpha}_2$ are shown in Fig. 7. They show similar pattern with $\hat{\alpha}_1$, which is natural for the two path channel simulation with the number of paths assumed known in the processing. Fig. 6(c) and Fig. 7(c) show that larger time delay difference enhances parameter resolution.

Fig. 8 shows a sample channel parameter estimate of the simulation. The new method successfully decomposes two paths although their channel parameter differences are merely a subfraction of the classical limit.

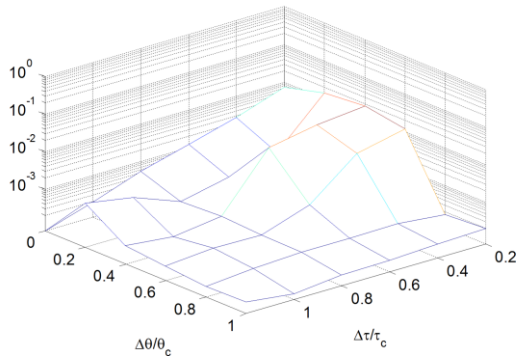

(a)

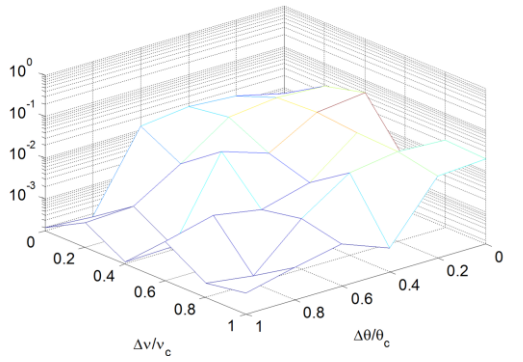

(b)

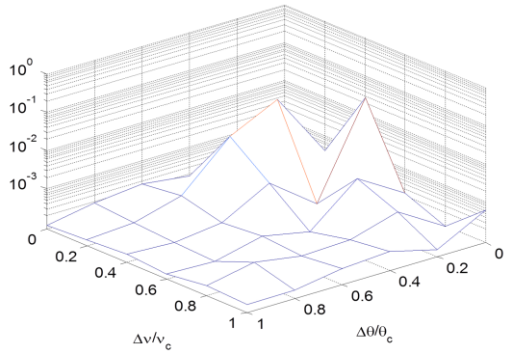

(c)

Fig. 6. RMSEE of $\hat{\alpha}_1$ as a function of (a) $\Delta\tau$ and $\Delta\theta$ with $\Delta\nu$ =0. (b) $\Delta\theta$ and $\Delta\nu$ with $\Delta\tau$ =0.2$\cdot\tau_c$. (c) $\Delta\theta$ and $\Delta\nu$ with $\Delta\tau = \tau_c$.

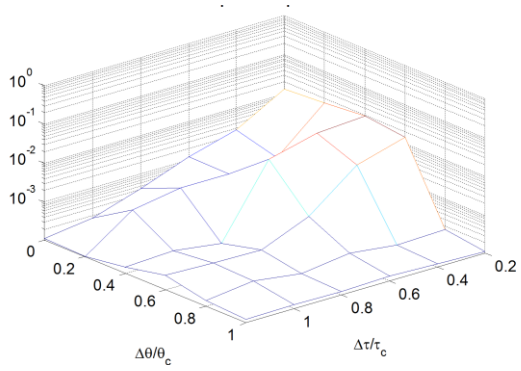

(a)

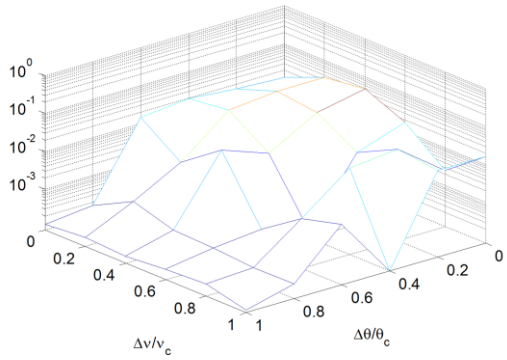

(b)

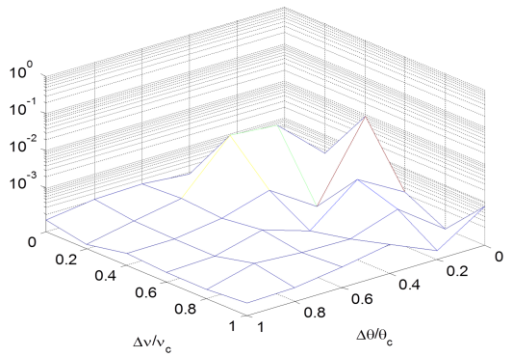

(c)

Fig. 7. RMSEE of $\hat{\alpha}_2$ as a function of (a) $\Delta\tau$ and $\Delta\theta$ with $\Delta\nu$ =0. (b) $\Delta\theta$ and $\Delta\nu$ with $\Delta\tau$ =0.2$\cdot\tau_c$. (c) $\Delta\theta$ and $\Delta\nu$ with $\Delta\tau=\tau_c$.

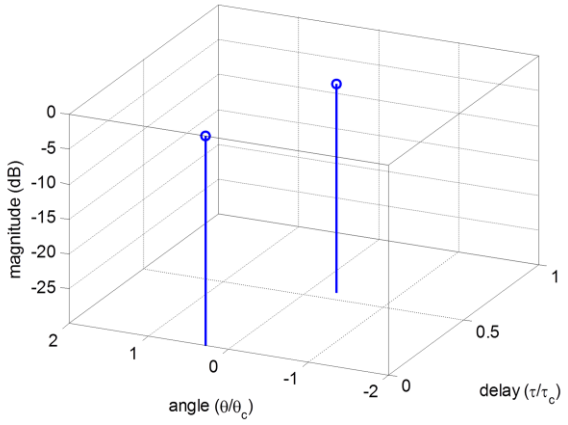

(a)

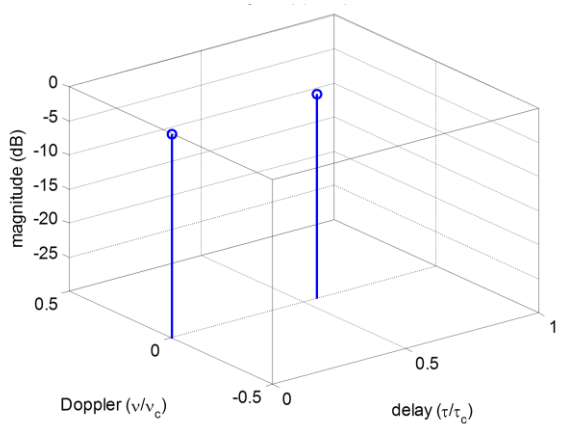

(b)

Fig. 8. A sample channel parameter estimate selected from the simulation result when $\Delta\tau = 0.6 \cdot \tau_c$, $\Delta\theta = 0.6 \cdot \theta_c$, and $\Delta\nu = 0 \cdot \nu_c$.

Chapter 4
Parameter Estimation of Real Channels

In this chapter, the results of the experimental data analysis are presented. The data were obtained from two different channels.

The first channel is a large scale water tank where the surface wave can be generated with designated wave parameters. As we know the surface wave parameters such as wave period, length and height, we can obtain the analytic solution of the channel parameters, and these can be used as the reference for performance evaluation.

The second channel to be analyzed is the shallow sea water channel which shows sparse signal transmission structure. In this case, we do not know the exact parameter values, and therefore the validity of the estimation results is evaluated indirectly using the channel characteristic functions which are indicative of channel parameters.

4.1 Water Tank Channel Experiment

The Ocean Engineering Basin (OEB), a water tank facility of MOERI/KIOST, is capable of generating a surface gravity wave with user-specified wave parameters, and therefore it provides the opportunity to get time-varying multipath channel data of a known channel environment.

We did a channel measurement experiment named as *OEB 2010* where a regular surface wave was generated with wave parameters given in Table VI. The pseudo-random noise (PN) signal was transmitted by an omnidirectional hydrophone (B&K 8105), and the transmitted signal was recorded by an eight-element hydrophone array. Fig. 9(a) shows the overview of the OEB, and Fig. 9(b) shows the transmitter (A) and receiver (C) positions of the experiment which were installed at interval of 5 m. The details of the experiment setup were summarized in Table VII. The transmitter and the receiver instrumentation is described in Fig. 10.

TABLE VI
SURFACE WAVE GENERATION IN *OEB 2010*

Wave condition	Period	Amplitude	Wavelength
WAVE 0	No wave	No wave	No wave
WAVE 2	1.5 sec	4 cm	3.51 m

TABLE VII
EXPERIMENT SETUP OF *OEB 2010*

Parameter	Value
Carrier frequency (f_c)	20 kHz
Symbol rate ($f_{sym} = 1 / T_{sym}$)	10 kHz
Pulse shaping filter	Root-raised-cosine filter (order = 20, rolloff factor = 1.00)
Number of array elements (M)	8
Array element spacing (d)	3 cm
Transmit signal	511 symbol PN sequence
Observation time window (T_w)	51.1 milliseconds ($= 511 \times T_{sym}$)
Transmitter-receiver range (m)	5.101 m
Transmitter depth	1.5 m
Receiver depth	1.1 m

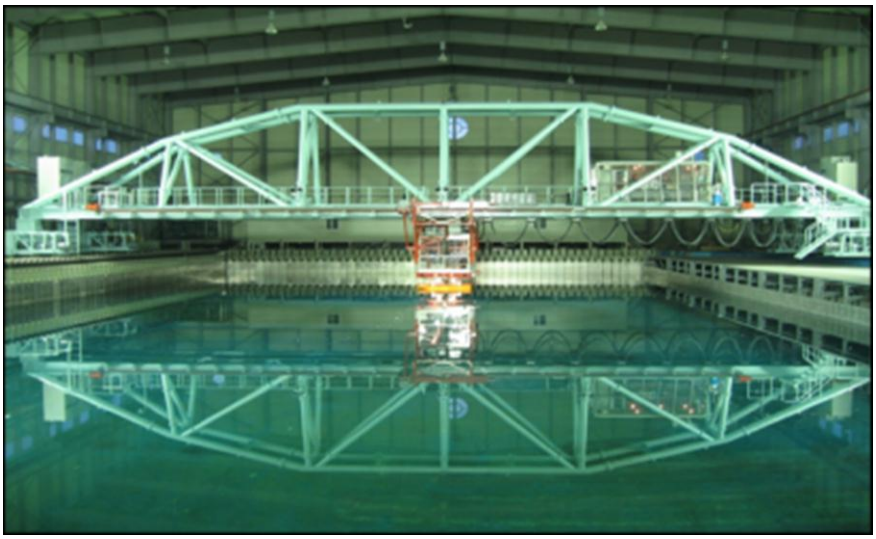

(a)

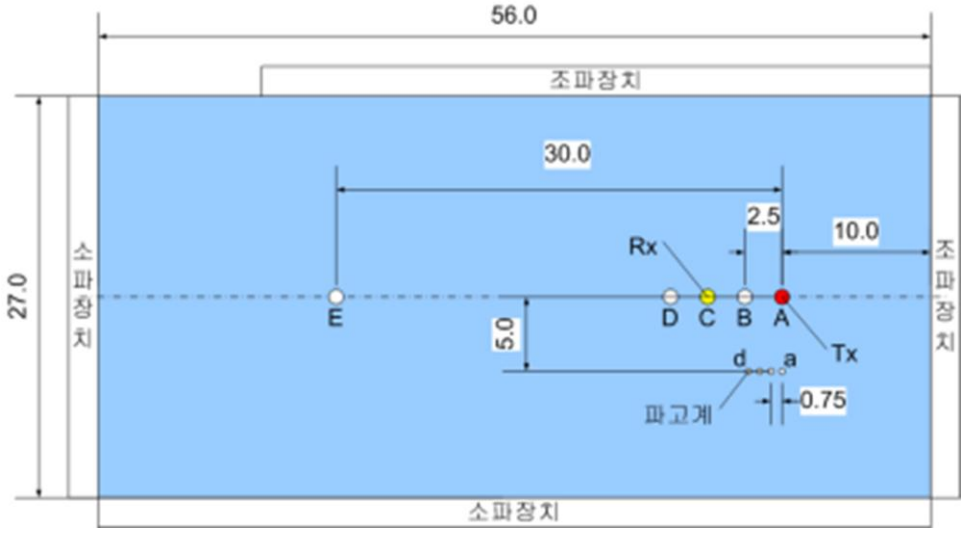

(b)

Fig. 9. (a) Panoramic view of the Ocean Engineering Basin at MOERI/KIOST and (b) Plan view of the transmitter and receiver positions.

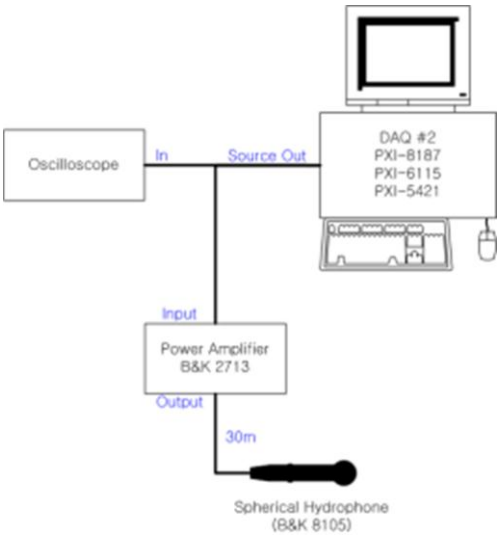

(a)

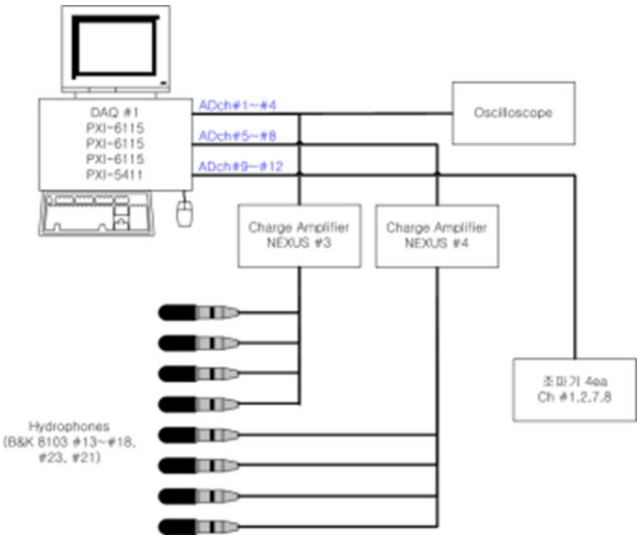

(b)

Fig. 10. (a) Transmitter and (b) Receiver used in *OEB 2010*.

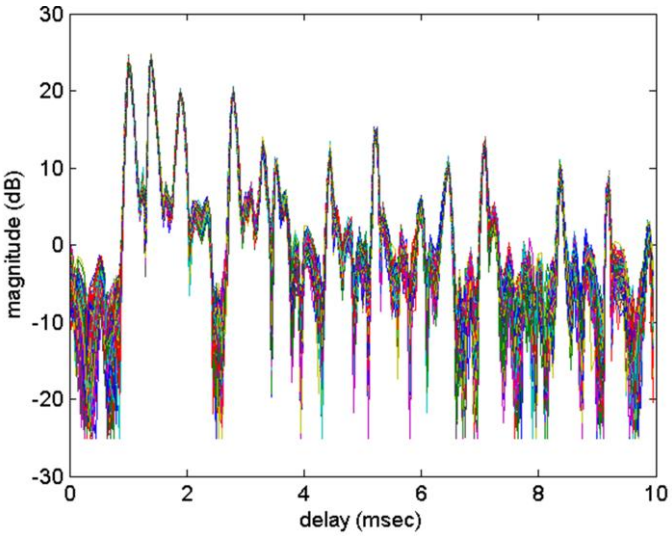

(a)

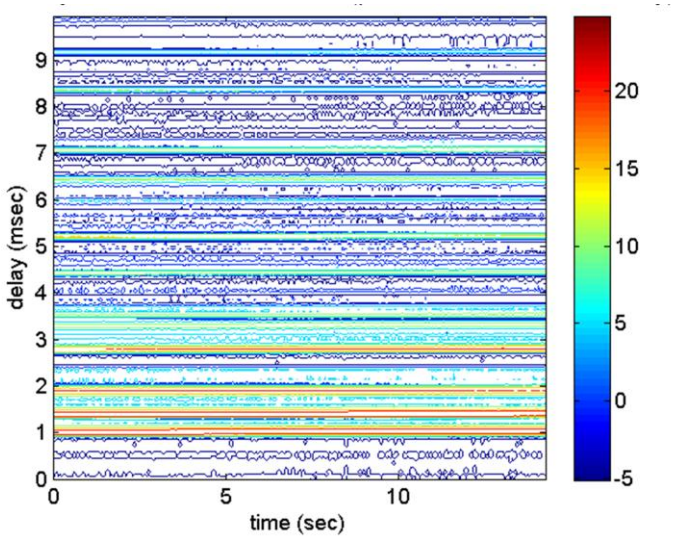

(b)

Fig. 11. The CIR's for WAVE 0. (a) The CIR's at different time blocks are overlaid all together and (b) the input delay-spread function.

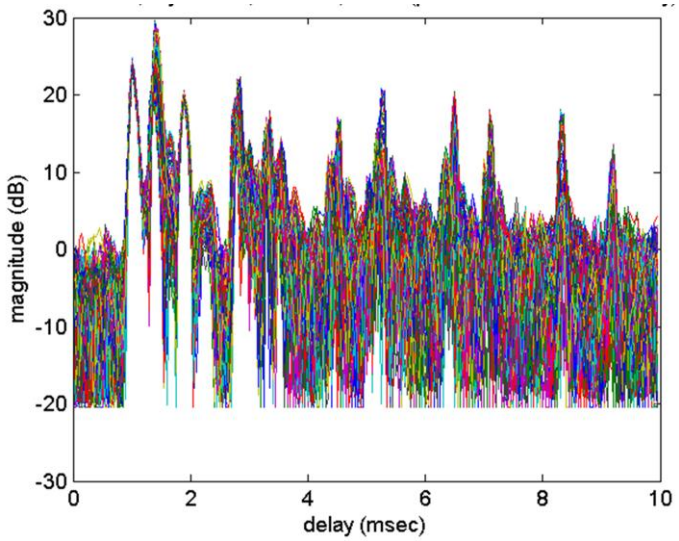

(a)

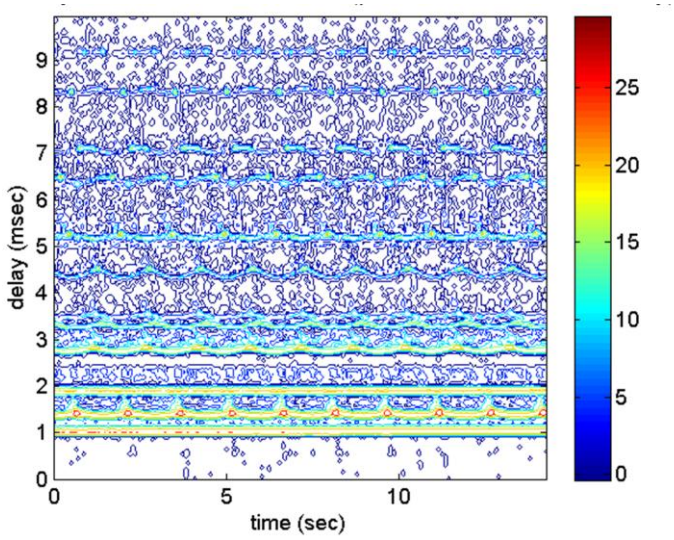

(b)

Fig. 12. The CIR's for WAVE 2. (a) The CIR's at different time blocks are overlaid all together and (b) the input delay-spread function.

The objective of the data analysis is to test whether the presented channel estimation algorithm can identify the multipath components under the time-varying surface wave in the water tank channel condition which is acoustically reverberant. The generated surface wave parameters are given in Table VI.

Before going into analysis of the time-varying case, we present the channel impulse response of no surface wave case (WAVE 0) in Fig. 11. Fig. 11(a) shows the channel impulse responses (CIR) for 10 seconds, and Fig. 11(b) shows the same result with plotted vs. time, i.e., the input delay-spread function. We can see that the channel variation over time is negligible and there exist a large number of multipaths caused by the reflections at the basin's surface and bottom boundaries. Fig. 12 shows the CIR's for WAVE 2 where the effect of the surface wave clearly can be seen.

4.1.1 Surface Reflected Signal Model

The signals reflected from the moving surface are usually obtained by ray tracing [43] but when the formula of the surface wave is known along with its wave parameters and if the ray bending caused by sound speed profile is negligible, we can obtain simple analytic solution of the time-varying channel parameters from the geometrical condition of surface reflection.

Fig. 13 shows the geometry of surface reflection. When the surface wave y_w is assumed sinusoidal as is given by

$$y_w = a\cos\left(\omega_w t - k_w x + \phi\right) \tag{4.1}$$

where ω_w is the frequency, k_w is the wave number, a is the amplitude, and ϕ is the phase offset of the surface wave. The surface grazing angle θ_i and the reflected angle θ_r must be same with respect to the surface tangential plane, i.e.,

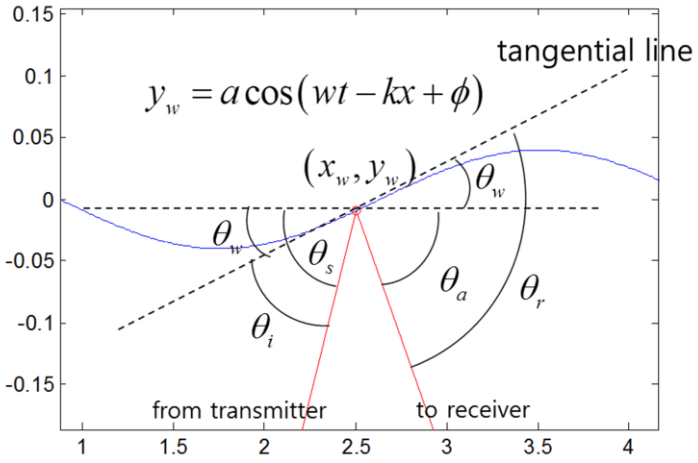

Fig. 13. The geometry of the surface reflection. (Angles are shown exaggerated due to unequal axis scale.)

$$\tan\theta_i = \tan\theta_r . \tag{4.2}$$

When the angle with respect to the horizontal line from the reflection point to the transmitter and the receiver are denoted as θ_s and θ_a, respectively, they are given by

$$\tan\theta_s \triangleq \frac{y_w - y_s}{x_w - x_s}, \tag{4.3}$$

$$\tan\theta_a \triangleq \frac{y_a - y_w}{x_a - x_w}, \tag{4.4}$$

$$\tan\theta_w \triangleq \frac{dy_w}{dx} = ak\sin(\omega t - kx) . \tag{4.5}$$

where θ_w is the angle between the horizontal line and the tangential line at the reflection point x_w. Then the angles are related as follows:

$$\theta_i = \theta_s - \theta_w , \tag{4.6}$$

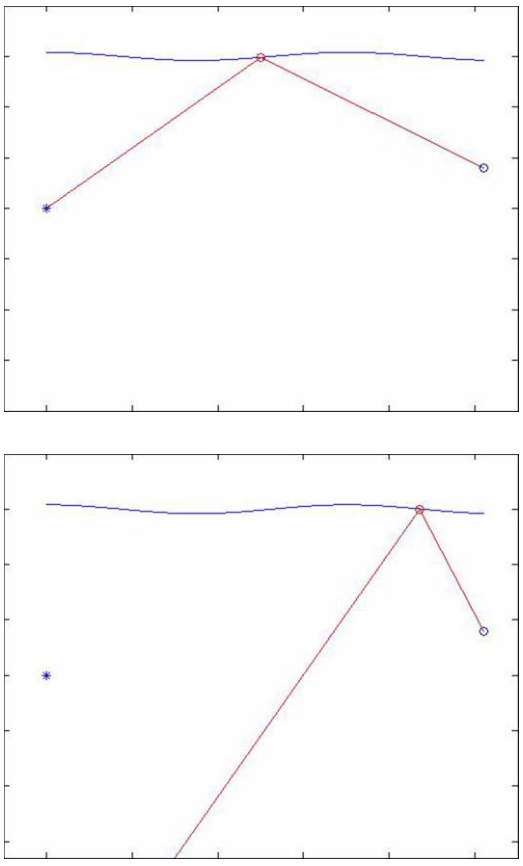

(a)

(b)

Fig. 14. Sample surface reflection path obtained by (4.8). The asterisk and the circle correspond to the transmitter and the receiver positions, respectively. (a) The surface reflected path and (b) the bottom-surface reflected path.

$$\theta_r = \theta_a + \theta_w, \tag{4.7}$$

Inserting (4.6) and (4.7) into (4.2) gives

$$\tan(\theta_s - \theta_w) = \tan(\theta_a + \theta_w). \tag{4.8}$$

Here, θ_s, θ_w, and θ_a are functions of x_w as given in (4.3)-(4.5). Therefore finding x_w satisfying (4.8) gives the possible reflection points x_w and the reflection angles can be

obtained by inserting x_w into (4.3) and (4.4). Sample paths obtained by such analytic method are given in Fig. 14. Fig. 14(a) and (b) show a sample of the surface reflected path and the bottom-surface reflected path, respectively. The bottom-surface reflected path can be solved by placing an image transmitter below the bottom with symmetry. Thus all the paths which bounce once at the air-water interface can be obtained by this method.

4.1.2 Comparison between Data and Model

Now we compare the channel estimation result with the analytic solution. In Fig. 15, the channel parameters obtained by the SAMP are shown. In the processing, 40 paths were assumed ($S = 40$). The parameter variation caused by the moving surface wave is evident. Fig. 15(a) shows the estimated time delays and Fig. 15(b) shows the estimated incidence angles. The incidence angle of the direct path is shown at the center of Fig. 15(b) and is shown constant because the direct path is not dependent on the surface wave motion. The above of the direct path show the angle of the surface reflected path, and those below the direct path shows the angle of the bottom reflected path which is also independent of the surface wave motion.

In Fig. 16(a), the incidence angle and Doppler shift of the surface reflected path by the analytic solution is shown, and those estimated by the SAMP are shown in Fig. 16(b). The estimated result coincides with the model except a constant phase offset which is caused by unknown initial phase of the generated surface wave. If the classical resolution limits which were given in Section 3.1 are considered, we can see that the SAMP shows high resolution performance both in angle and Doppler shift estimation. The classical limits for the *OEB 2010* data are given by

$$\tau_c = T_{sym} = 0.1 \ (\text{ms}), \quad \theta_c = \frac{2}{M} = 0.25 \ (\text{rad}), \text{ and } \quad \nu_c = \frac{1}{T_w} = 19.57 \ (\text{Hz}),$$

and angles whose differences are below θ_c were successfully decomposed as shown in Fig.

15 and Fig. 16. Fig. 17 gives the comparison result of the incidence angle and the time delay. All plot symbols indicates equispaced time sample. Therefore wider spacing of the time delay near the local minimum and maximum points of the incidence angle implies that the magnitude of Doppler shift becomes maximal at those points. This is in accordance with the result given in Fig. 16 where the Doppler shift was shown similar to the reverse of the incidence angle.

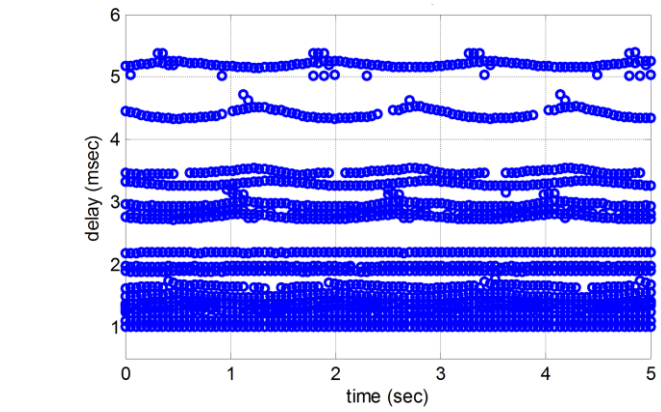

(a)

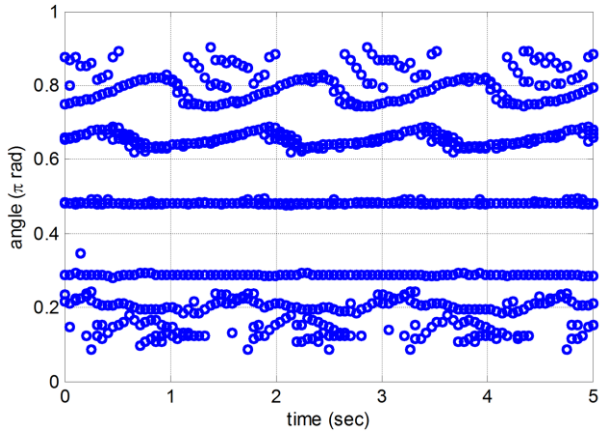

(b)

Fig. 15. Estimated channel parameters by the SAMP. (a) Time delay vs. time and (b) incident angle vs. time

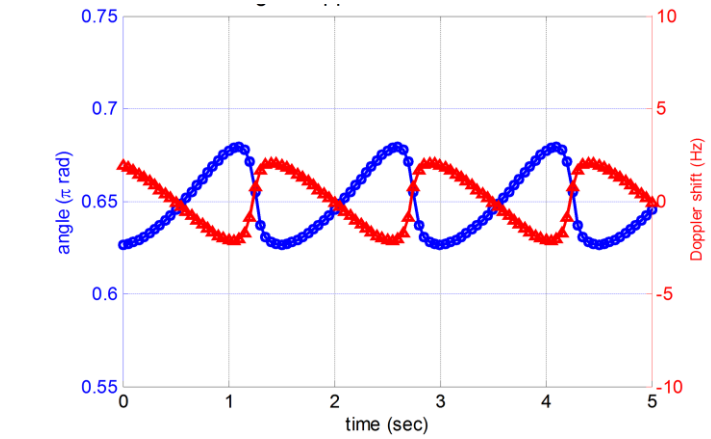

(a)

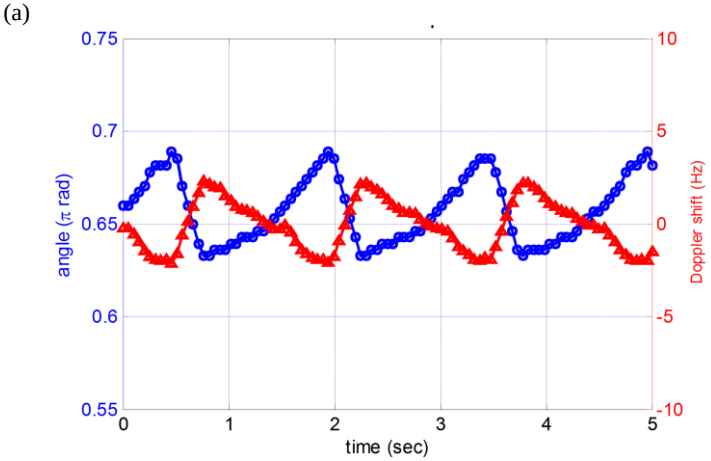

(b)

Fig. 16. Comparison of incidence angle and Doppler shift between (a) Model and (b) channel estimation. The circle (blue) is the incidence angle, and the triangle (red) is the Doppler shift.

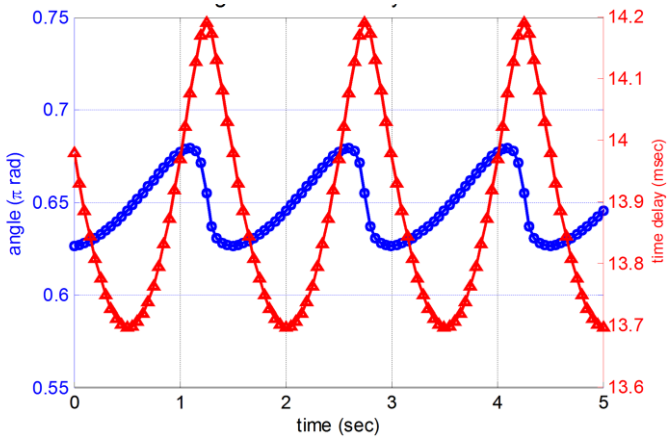

(a)

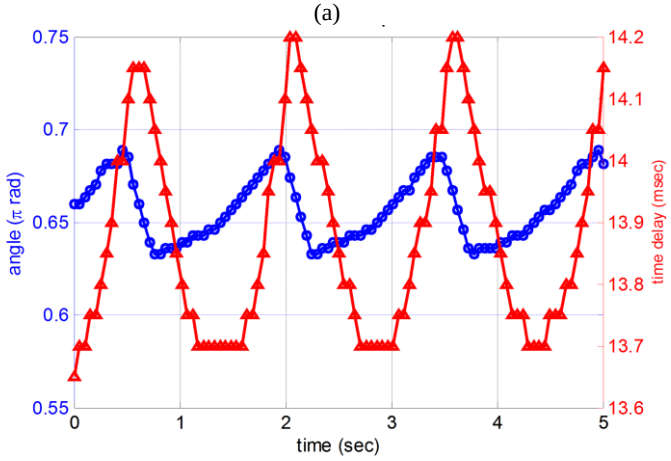

(b)

Fig. 17. Comparison of incidence angle and time delay between (a) Model and (b) channel estimation. The circle (blue) is the incidence angle, and the triangle (red) is the time delay.

4.2 Shallow Water Channel Experiment

In this section, we demonstrate the performance of the SAMP by applying it to the channel measurement data obtained from the shallow water. Because the true channel parameters are not known, the performance evaluation is carried out through the comparison of channel characteristic functions synthesized from the estimated parameters with those computed from the measurement data.

We use *Jangmok 2008* experiment data which were gathered from Jinhae bay where the water depth was about 21 m and small-scale surface wave existed (Fig. 18). An omnidirectional transducer was used as the transmitter and an eight-element vertical array of 6

(a)

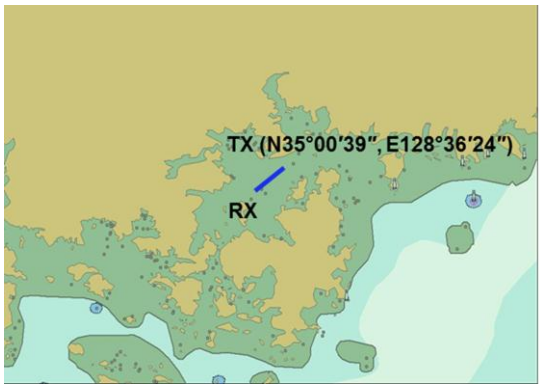

(b)

Fig. 18. The location of *Jangmok 2008* channel measurement experiment. (a) Location of Jinhae bay and (b) enlarged view of experiment location.

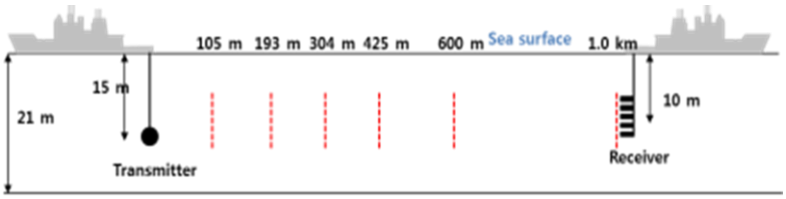

Fig. 19. Experiment setup of *Jangmok 2008.*

TABLE VIII
EXPERIMENT SETUP OF *JANGMOK 2008*.

Parameter	Value
Carrier frequency (f_c)	25 khz
Symbol rate ($f_{sym} = 1/T_{sym}$)	10 khz
Pulse shaping filter	Root-raised-cosine filter (order = 20, rolloff factor = 0.35)
Number of array elements (M)	8
Array element spacing (d)	One wavelength (unambiguous angle = [$\frac{\pi}{3}$ $\frac{2\pi}{3}$])
Transmit signal	255 symbol pn sequence
Observation time window (T_w)	25.5 milliseconds ($= 255 \times T_{sym}$)
Time delay interval (N_τ)	40 samples per symbol period
Angle interval (N_θ)	256 samples per angle range
Doppler shift interval (N_v)	256 samples per Doppler shift range [-39 39] (Hz)
Transmitter-Receiver range (m)	105, 193, 304, 425, 600, 1000

cm element spacing was used to receive the transmitted signal. The signals were gathered at ranges: 0.1, 0.2, 0.3, 0.4, 0.6, and 1.0 km. Fig. 19 describes the experiment setup of *Jangmok 2008*. The signals were sampled at 200 ksps and recorded for 10 seconds. The experiment parameters are summarized in Table VIII.

Fig. 20 shows the input delay-spread functions of the uppermost array element at all ranges. The input delay-spread function is the matched filter response which is obtained by cross correlating the received signal of an interested duration with the transmit signal. Thus it is equivalent to the time-varying channel impulse responses. The sparse structure of the shallow water channel and the time variability caused by the surface gravity wave clearly can be seen. As the transmitter-receiver range increases, the number of dominant paths tends to increase whereas the time delay difference among the paths decreases. At 0.6 km range in Fig.

20(e), the SNR of the received signal was peculiarly low.

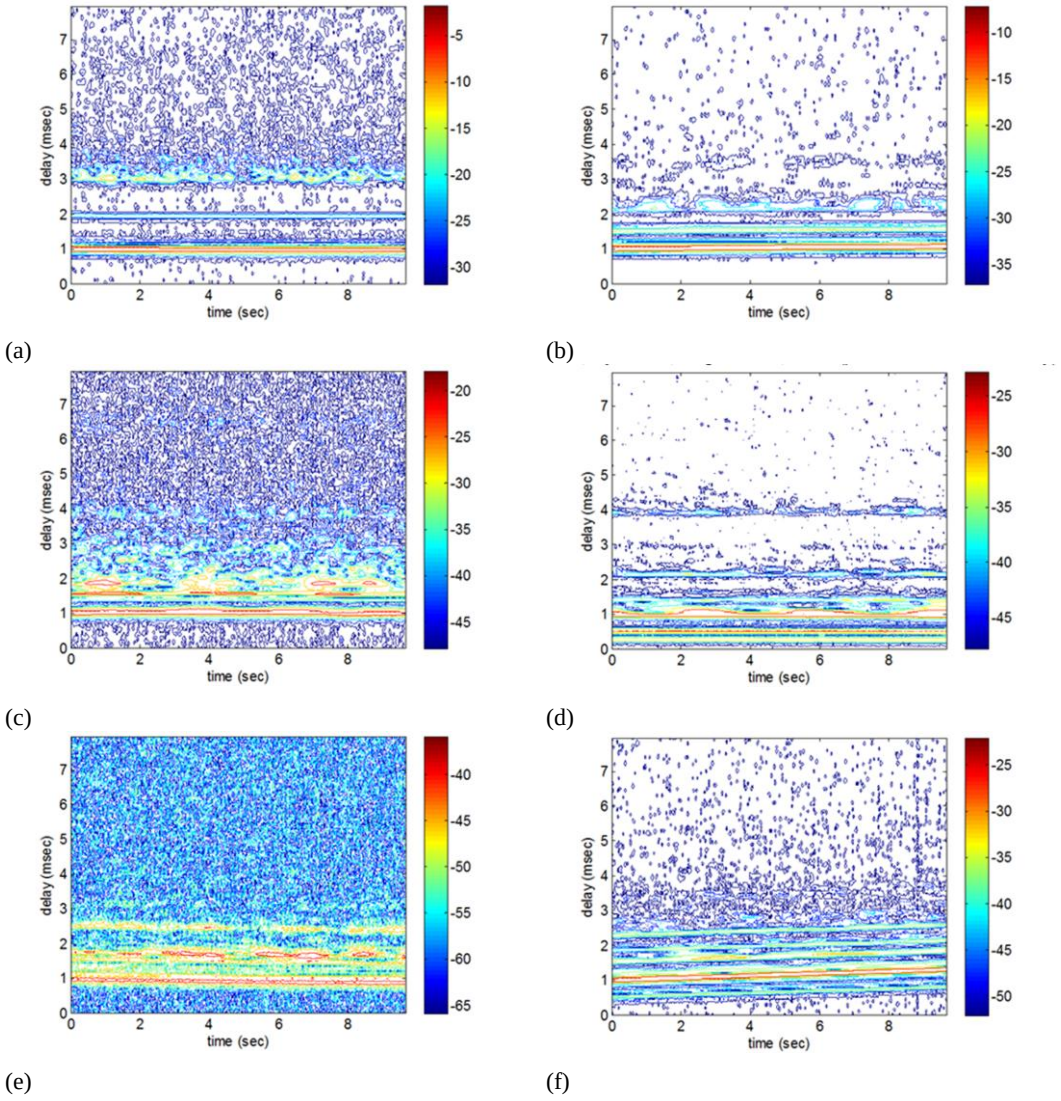

Fig. 20. The input delay-spread function obtained at the first channel using the matched filter. The transmitter-receiver ranges are (a) 105 m, (b) 193 m, (c) 304 m, (d) 425 m, (e) 600 m, and (f) 1000 m.

4.2.1 Estimation of Incidence Angle

In Fig. 21, the estimation results for 0.1 km range by the SAMP and those by the matched filter with the wideband beamformer are shown. As shown in Fig. 21(a), there are three dominant path clusters at 0.1 km range which are the direct, the bottom bounce and the surface bounce paths in ascending time delay order. Whereas both the direct and the bottom bounce paths are represented by one dominant path (with relatively small diffusive multipath components for the direct path), the surface bounce path is represented by a few paths of similar power with a dozen of small-magnitude paths showing the surface scattering effect. To prove how well the SAMP method captures the parameters of superimposed multipath signals, we define the marginal angle-delay-spread function $g_\theta[k]$ as

$$g_\theta[k] \triangleq g\left[j_{\max}(k), k\right] \tag{4.9}$$

where $j_{\max}(k)$ is the incidence angle index for which $g[j,k]$ is maximized, i.e.,

$$j_{\max}(k) = \arg\max_j \left| g[j,k] \right|. \tag{4.10}$$

Because $g_\theta[k]$ implies the maximum magnitude of the multipath components impinging at the *k*th delay bin, it can be used as the reference for evaluating the estimation result. Fig. 21(b) shows the marginal angle-delay-spread function at 0.1 km range and the paths obtained by the SAMP are overlaid on it. The multipath components by the SAMP algorithm are in good agreement with the marginal angle-delay-spread function supporting that all the dominant multipath components are picked up by the SAMP in the time delay domain. In order to test the angle estimation performance of the SAMP, the angle-delay-spread function is computed. The angle-delay-spread function is the matched filter response of the wideband beamformer output [41] which shows power distribution of the impinging acoustic signal in the angle-delay axis. It is expressed as

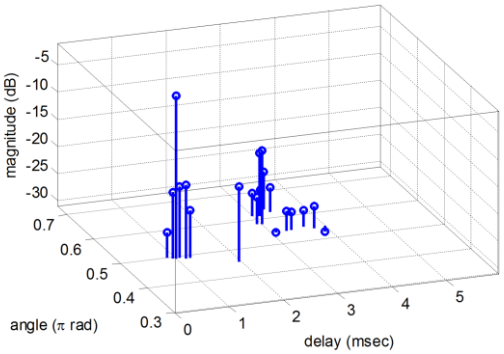

(a)

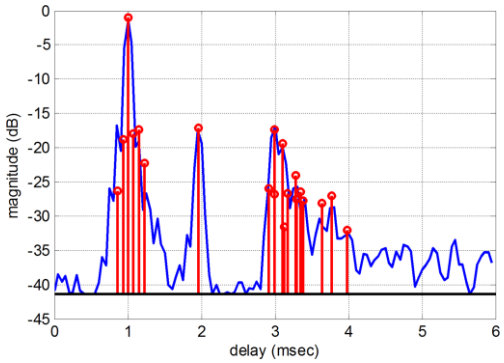

(b)

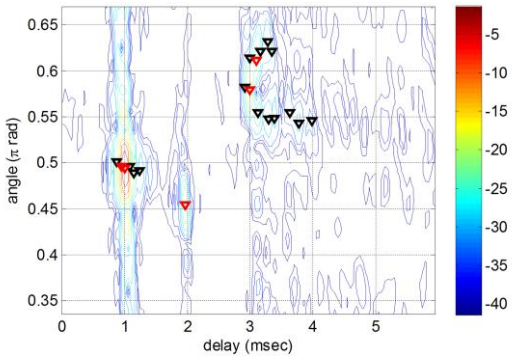

(c)

Fig. 21. Comparison of the SAMP with the angle-delay-spread function for range 105 m. (a) Estimated channel parameters by the SAMP. (b) The marginal angle-delay-spread function on which the results of the SAMP (circle) are overlaid. (c) The angle-delay-spread function on which the results of the SAMP are overlaid (triangle). The five strongest paths are shown in red.

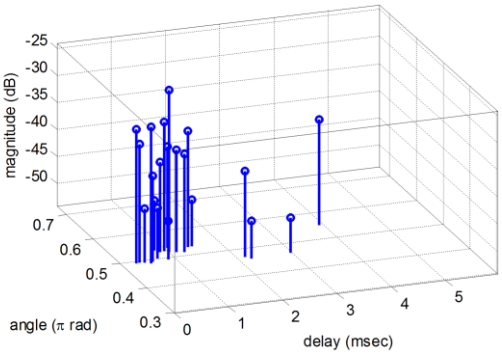

(a)

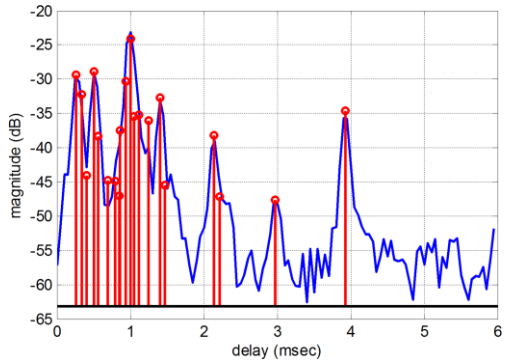

(b)

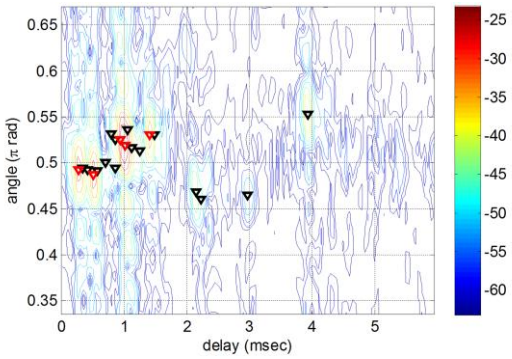

(c)

Fig. 22. Comparison of the SAMP with the angle-delay-spread function for range 425 m. (a) Estimated channel parameters by the SAMP. (b) The marginal angle-delay-spread function on which the results of the SAMP (circle) are overlaid. (c) The angle-delay-spread function on which the results of the SAMP are overlaid (triangle). The five strongest paths are shown in red.

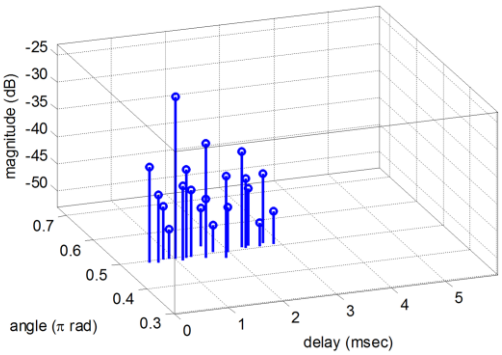

(a)

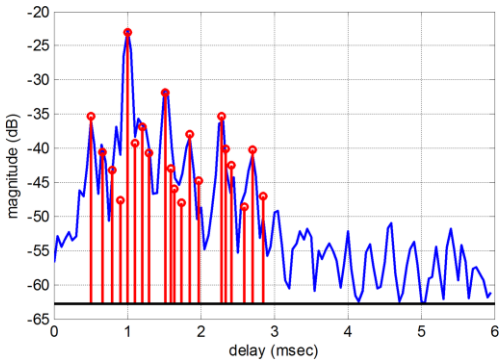

(b)

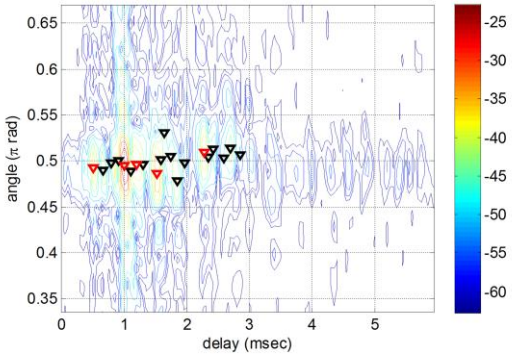

(c)

Fig. 23. Comparison of the SAMP with the angle-delay-spread function for range 1000 m. (a) Estimated channel parameters by the SAMP. (b) The marginal angle-delay-spread function on which the results of the SAMP (circle) are overlaid. (c) The angle-delay-spread function on which the results of the SAMP are overlaid (triangle). The five strongest paths are shown in red.

$$g[j,k] = \sum_{k'} y_{bf}[j,k']s^*[k'-k]. \qquad (4.11)$$

where $y_{bf}[j,k]$ is the jth beam signal at the kth time sample.

In Fig. 21(c), the angle-delay-spread function for the same range is shown along with the SAMP result. Exact contour peaks of the matched filter result are picked up by the SAMP algorithm. Fig. 22 and Fig. 23 show the results for 0.4 km and 1.0 km ranges, respectively. As shown in the figures, the results of the SAMP also coincide with the matched filter output proving its validity at long ranges. In general, it is thought that the channel parameter estimation is more difficult at long ranges because of smaller channel parameter differences. The differences of time delay and incidence angle among multipath components reduce with increasing range because of the waveguide effect which geometrically reduces the path differences at long range and attenuates the paths of large grazing angles. This can be easily confirmed by comparing the estimated time delay and incidence angle at different ranges shown in Fig. 21 to Fig. 23.

4.2.2 Estimation of Doppler Shift

The signal model suggested in Section 2.1 takes into consideration the time variability of the channel and is equivalent to the first order approximation in that it considers the phase variation by Doppler shift as expressed in (2.5) but it neglects the signal compression or dilation which is probable for underwater acoustic communication channel due to the low propagation speed of sound. However, when the speed of a platform or surface wave movement is not excessive, the compression/dilation effect is negligible so that the model fits well with real channel response. The accuracy of Doppler shift estimation by the SAMP is evaluated in the same way as the incidence angle treated in the previous section. The delay-Doppler-spread function, which is the Fourier transform of the input delay-spread function, is used for evaluating the SAMP results. It is analogous to the angle-delay-spread function used

in the incidence angle evaluation. The marginal delay-Doppler-spread function $g_\nu[k]$ is also defined in the same manner with (4.9) but now $j_{\max}(k)$ represents the Doppler shift index for which the delay-Doppler-spread function is maximized at time index k.

Fig. 24(a) shows the time delay and Doppler shift estimated by the SAMP algorithm for 0.1 km range data. Because of negligible platform motion and sea surface movement, the Doppler shifts are almost zero, and this is also observed in the delay-Doppler-spread function computed at the same recording time shown in Fig. 24(c). $g_\nu[k]$ and the SAMP result for 0.1 km range are shown in Fig. 24(b) where the peaks of $g_\nu[k]$ are well matched to the SAMP result. In other words, the most dominant path among the paths of different Doppler shifts but of the same time delay is picked up by the SAMP algorithm, and their magnitudes are consistent with the SAMP result. Fig. 25 and Fig. 26 are the results of 0.4 km and 1.0 km ranges, respectively, and they also support that the SAMP gives consistent Doppler shift estimation with the delay-Doppler-spread function.

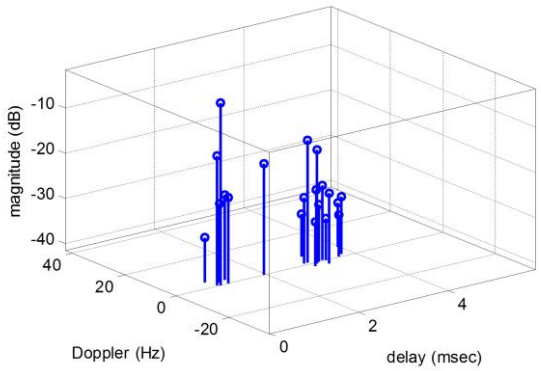

(a)

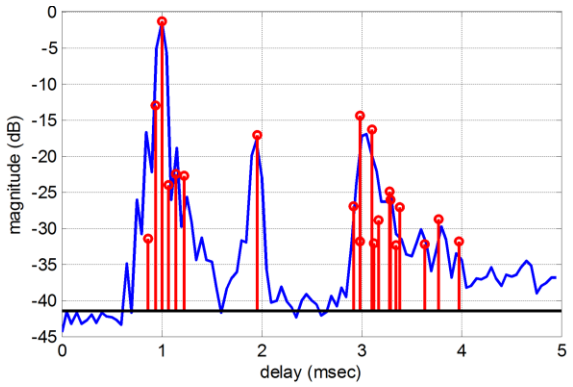

(b)

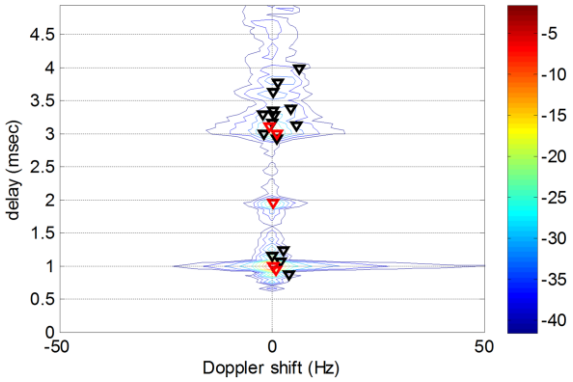

(c)

Fig. 24. Comparison of the SAMP with the delay-Doppler-spread function for range 105 m. (a) Estimated channel parameters by the SAMP (b) The marginal delay-Doppler-spread function on which the results of the SAMP (circle) are overlaid (c) The delay-Doppler-spread function with the results of the SAMP are overlaid (triangle). The five strongest paths are shown in red.

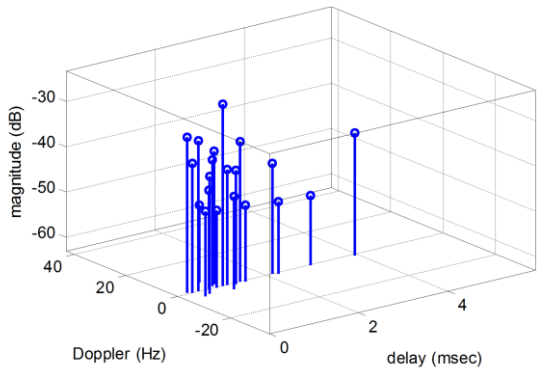

(a)

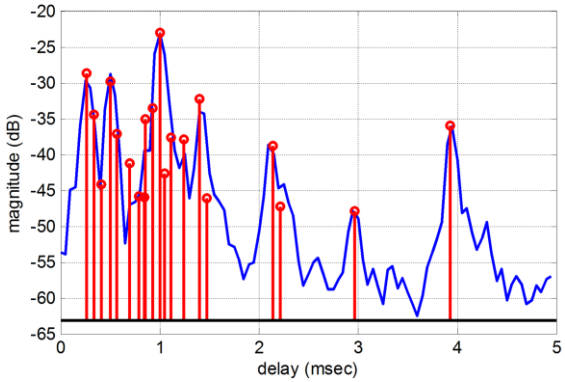

(b)

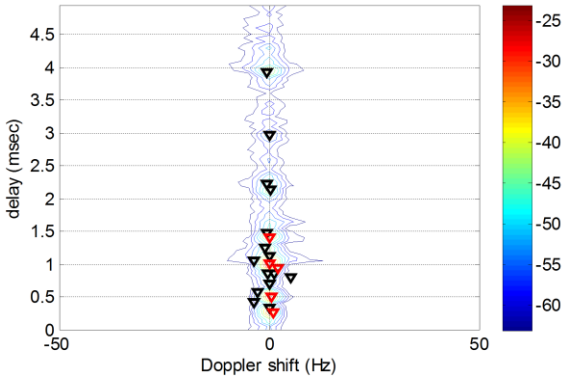

(c)

Fig. 25. Comparison of the SAMP with the delay-Doppler-spread function for range 425 m. (a) Estimated channel parameters by the SAMP (b) The marginal delay-Doppler-spread function on which the results of the SAMP (circle) are overlaid (c) The delay-Doppler-spread function with the results of the SAMP are overlaid (triangle). The five strongest paths are shown in red.

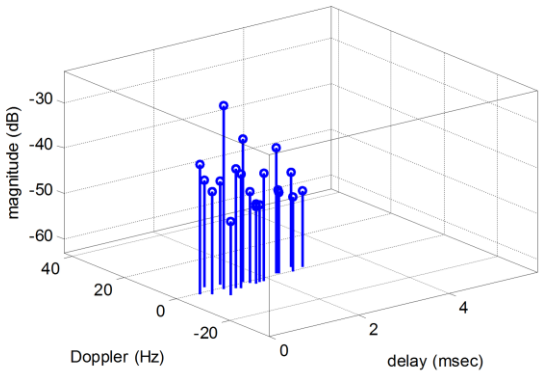

(a)

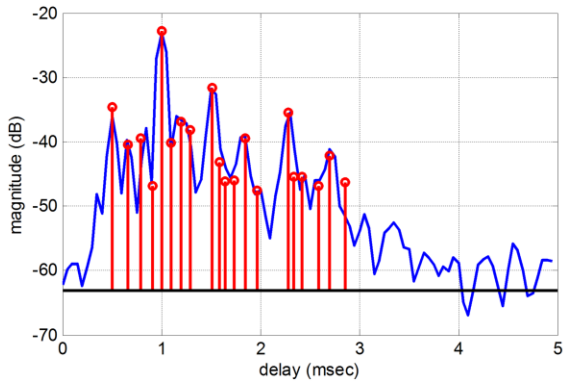

(b)

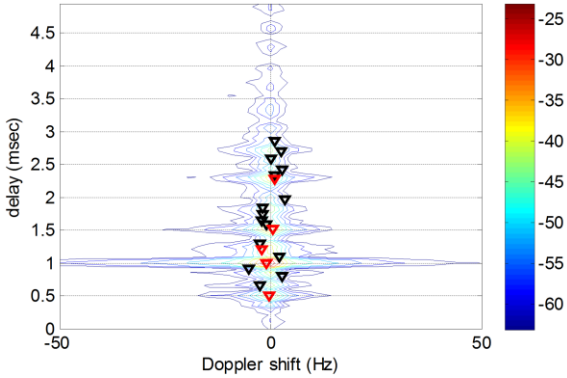

(c)

Fig. 26. Comparison of the SAMP with the delay-Doppler-spread function for range 1000 m. (a) Estimated channel parameters by the SAMP (b) The marginal delay-Doppler-spread function on which the results of the SAMP (circle) are overlaid (c) The delay-Doppler-spread function with the results of the SAMP are overlaid (triangle). The five strongest paths are shown in red.

4.2.3 Delay and Angle Profiles

In order to verify the presented algorithm further, we compute the power delay profile (PDP) and the power angle profile (PAP) of the signal reconstructed by the estimated parameters and compare them with those of the measured signal. This corresponds to the fifth evaluation criterion introduced in Section 3.1. If the estimated parameters are consistent with the true parameters, the PDP's and PAP's of both signals must coincide for the level above the noise floor.

In this theme, the PDP $P_{D,z}[k]$ and the PAP $P_{A,z}[j]$ of a signal z are defined as

$$P_{D,z}[k] \triangleq \sum_j P_z[j,k], \tag{4.12}$$

$$P_{A,z}[j] \triangleq \sum_k P_z[j,k], \tag{4.13}$$

where $P_z[j,k]$ is the magnitude square of the angle-delay-spread function of the signal which is given as

$$P_z[j,k] = \left| g_z[j,k] \right|^2 . \tag{4.14}$$

Here, $g_z[j,k]$ is defined by (4.11). Therefore, the PDP and the PAP implies the power distribution over time delay and incidence angle, respectively. If the reconstructed signal is represented in vector form as given z by

$$\mathbf{z} = \left[z[i] \quad z[i-1] \quad \cdots \quad z[i-I+1] \right]^T , \tag{4.15}$$

Then it is expressed by the SAMP result from Table II as

$$\mathbf{z} = \mathbf{U}_S \mathbf{x}_S . \tag{4.16}$$

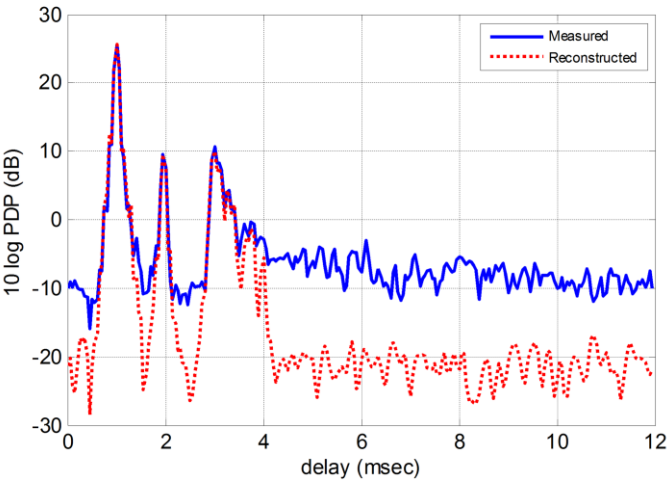

(a)

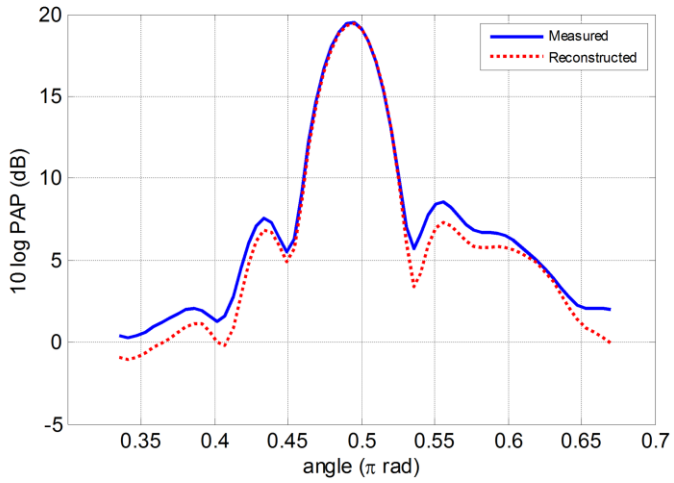

(b)

Fig. 27. Comparison of the power profile of the measured and the synthesized signals at range 105 m: (a) Power delay profile (PDP) and (b) Power angle profile (PAP).

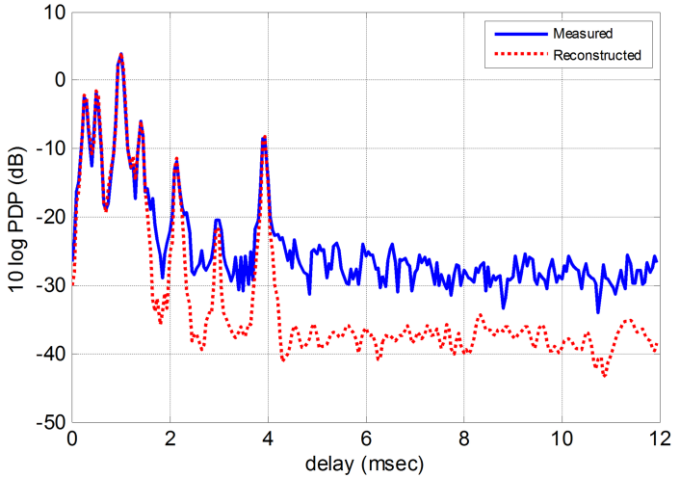

(a)

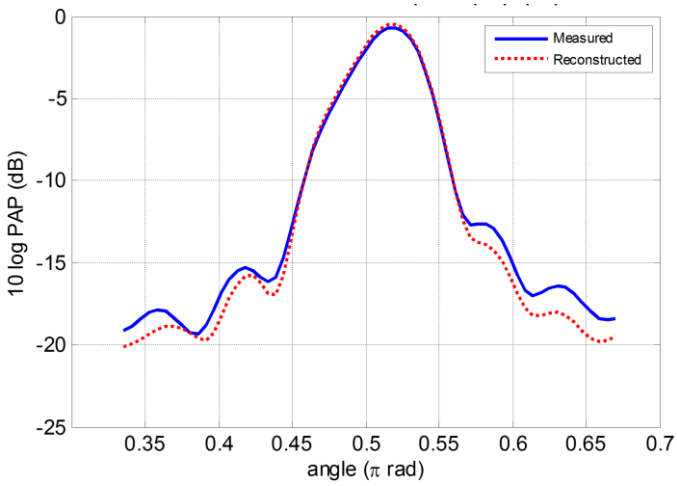

(b)

Fig. 28. Comparison of the power profile of the measured and the synthesized signals at range 425 m: (a) Power delay profile (PDP) and (b) Power angle profile (PAP).

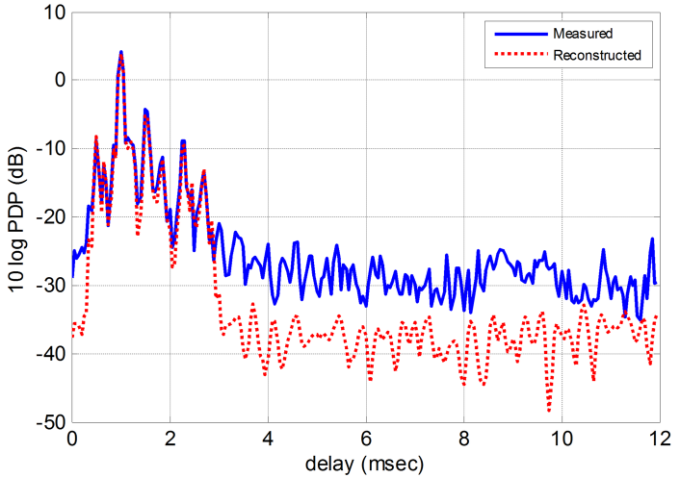

(a)

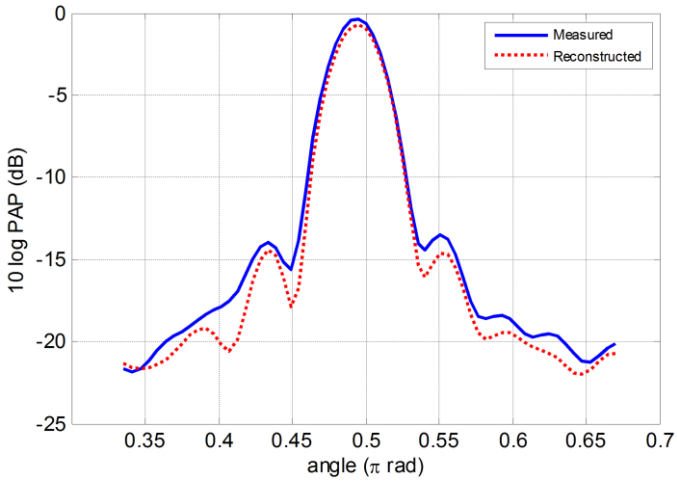

(b)

Fig. 29. Comparison of the power profile of the measured and the synthesized signals at range 1000 m: (a) Power delay profile (PDP) and (b) Power angle profile (PAP).

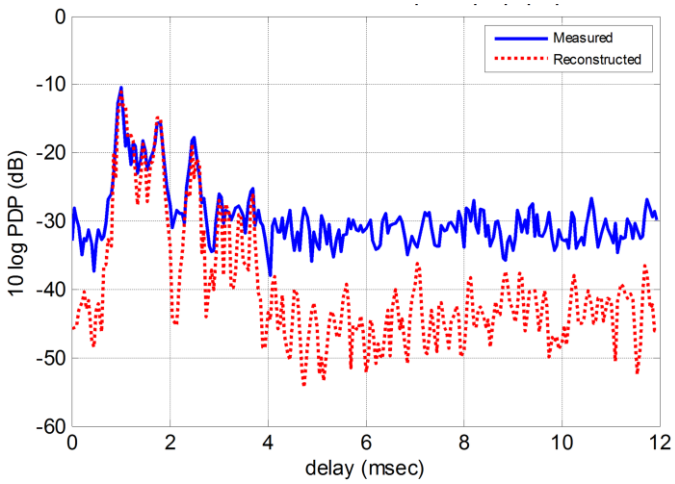

(a)

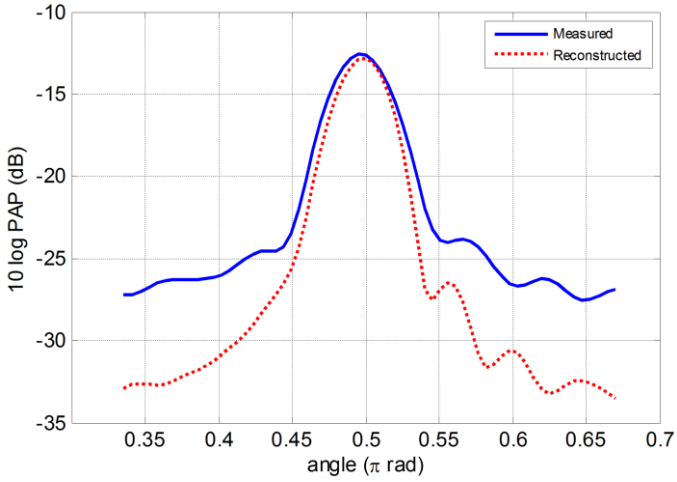

(b)

Fig. 30. Comparison of the power profile of the measured and the synthesized signals at range 600 m: (a) Power delay profile (PDP) and (b) Power angle profile (PAP).

where $\mathbf{U}_S$ is the dictionary whose columns were selected by the SAMP and therefore its column size is S.

The power profiles of the measured and the reconstructed signals at 0.1, 0.4 and 1.0 km ranges are given in Fig. 27 to Fig. 29. Twenty paths are used for reconstruction, i.e., *S*=20 in (4.16). In all ranges given, the PDP of the reconstructed signal coincides with the measured signal until -25 dB below the maximum level and this proves that the reconstructed signal has almost identical multipath structure in time delay. Similarly, the PAP of the reconstructed signal is in good agreement with that of the measured signal but the coincidence limit is -12 dB below the maximum level which is higher than the PDP. This higher discrepancy of the PAP is due to relatively low resolution in the angular domain which results in leakage and noise contribution from adjacent angle bins.

At 0.6 km range, the SNR was peculiarly lower than other cases (see Fig. 20). Accordingly, the differences of the power profiles are more pronounced as shown in Fig. 30. The difference is especially large when the magnitude becomes similar to the noise level as exemplified from 3 to 4 seconds in the time delay of the PDP and when the incident angle is outside of $[0.45\pi \;\; 0.53\pi]$ in the PAP. This large deviation is due to the low SNR which is evident in the PAP comparison. However, the overall features characterized by dominant paths are still well described by the reconstructed signal as can be seen in the PDP comparison.

Fig. 31 shows the residual signal energy variation at all ranges over the assumed number of paths which equals the number of iteration for the SAMP method. They are normalized by the received signal energy so that they are 0 dB (not shown) at the zero paths at which no signal is cancelled from the received signal. The residual signal energy consistently decreases with increasing number of paths because more signal components are cancelled from the residual signal. However, the amount of the residual reduction decreases as the iteration progresses. As shown in the figure, approximately after 30 iterations, the residual signal energy becomes saturated so that the residual levels are within about 1 dB of the minimum level of each case. The residual signal level is shown particularly high at 0.6 km range

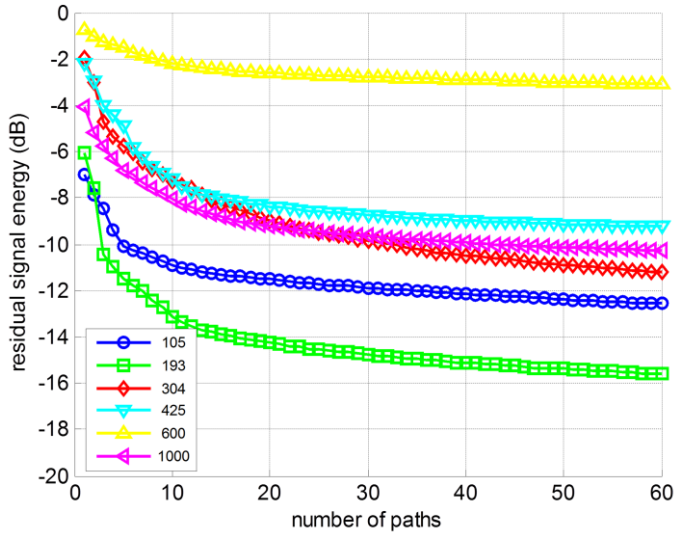

Fig. 31. Residual signal energy variation of the SAMP vs. the number of paths at all ranges.

because the input SNR is very low at that range. Fig. 31 also shows that the residual signal energy reduction is more pronounced at 0.1 and 0.2 km ranges. This is physically reasonable because lower SNR and higher level of diffusive path components scattered by the waveguide boundary and the medium inhomogeneity degrade the channel sparsity at long ranges.

Fig. 32 shows the arrival time delay vs. time at range 0.1 km. The input delay-spread function is shown in Fig. 32(a), and the paths identified by the SAMP were shown in Fig. 32(b). As discussed earlier, it shows that the surface bounce path has complicated pattern which is generated by interaction with the surface movement. The surface wave has more influence on the signal transmission at close range cases because the ratio of surface wave height to acoustic wavelength becomes larger than that of long range. This fact is evident if it is compared with 1.0 km range case given in Fig. 33(a). Both data were acquired in the same day with about three hour time lag so that the environmental condition is thought to be similar. But the dominant paths in Fig. 33(a) show more discrete and stable structure compared with 0.1 km case. Fig. 32(b) and Fig. 33(b) show the time delay estimation by the SAMP algorithm for each range. Twenty discriminated paths are shown and the five strongest paths among

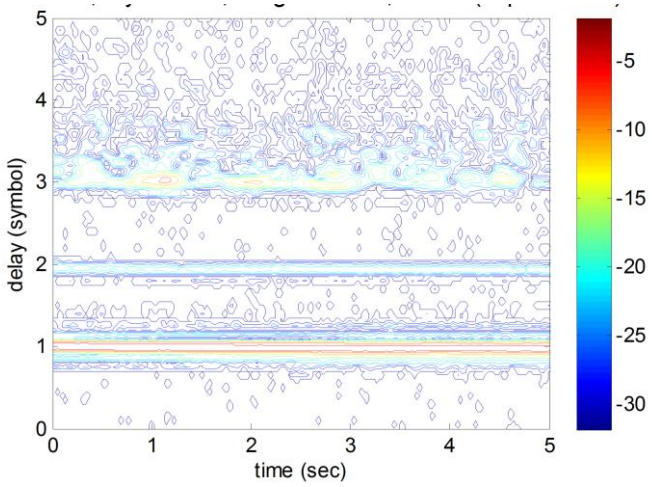

(a)

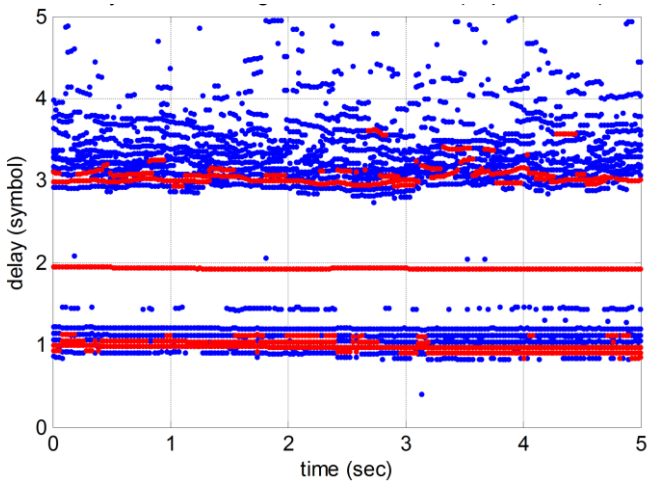

(b)

Fig. 32. Arrival time delay variation at range 105 m: (a) the input delay-spread function (enlarged) (b) time delay estimation by the SAMP algorithm. Twenty paths are shown in blue and the five strongest paths are marked in red.

them are marked in red. The results by the SAMP algorithm coincide with the input delay-spread functions in Fig. 32(a) and Fig. 33(a), and this proves the good channel tracking capability of the SAMP algorithm. It is noticed that the SAMP identifies weak paths which were not revealed by the input delay-spread function shown in the upper figure. This is well

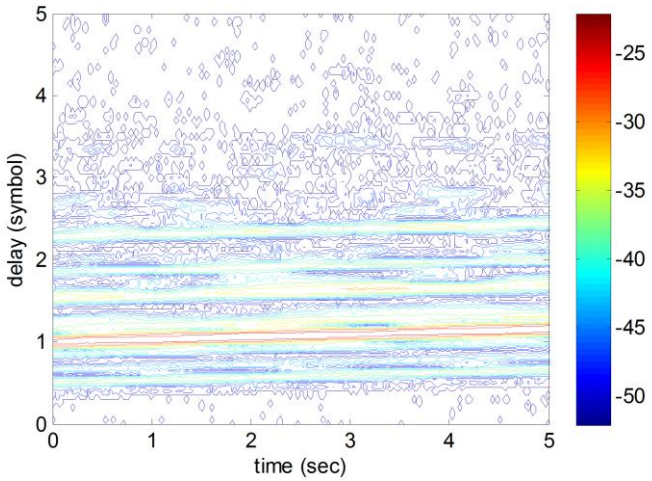

(a)

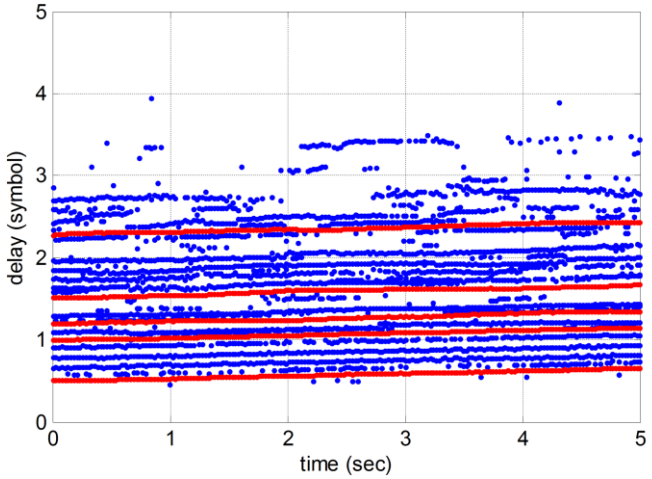

(b)

Fig. 33. Arrival time delay variation at range 1000 m: (a) the input delay-spread function (enlarged) (b) time delay estimation by the SAMP algorithm. Totally twenty paths are shown in blue and the five strongest paths are marked in red.

described by the paths whose time delays are between 2.5 and 3 milliseconds.

Chapter 5
Conclusions

We have addressed the sparse underwater acoustic communication channel estimation problem using a multichannel receiver array and developed new method which is based on the greedy algorithm. The contributions made in this thesis are summarized as follows:

First, we formalized the time-varying sparse channel estimation using a receiver array as the linear inverse problem as presented in Section 2.1. The derived inverse problem is based on the angle-delay-Doppler-spread function which is a natural extension of the delay-Doppler-spread function and allows sparse representation of the received signal using more generalized parameter set including the incidence angle. In addition, we showed that using a redundant dictionary of oversampled parameter range reduces the ambiguity of channel parameter estimation.

To exploit the sparse nature of the angle-delay-Doppler function, we presented a new greedy algorithm which enables a redundant dictionary to be used for precise parameter estimation. It overcomes difficulties of using large dimensional redundant dictionary by introducing the two stage processing scheme which utilizes the space-alternating iterative estimation. The proposed algorithm reduces the dimension of the dictionary and enables search over large dimensional parameter space with practical computation resources. This is the second contribution of this work.

The performance of the presented method was evaluated via numerical simulation and experimental data analysis. The numerical simulation showed high resolution performance of the presented algorithm by decomposing two paths of similar parameter values. We performed the channel estimation experiment under artificially generated surface wave in the large sized water tank. In particular, we presented the analytic solution of the channel parameters and used it to prove the consistency of the channel estimation result. This is the third contribution of this thesis. The analysis of the shallow sea water channel experiment data

showed that the presented algorithm gives reasonable channel estimation result for the real channels. However, the mathematical conditions for the presented algorithm to give optimal estimation were not rigorously handled, and its validity was proved rather heuristically using numerical simulation and experimental data analysis. This leaves an important issue for future research.

References

[1] F. B. Jensen, W. A. Kuperman, M. B. Porter, and H. Schmidt, *Computational ocean acoustics*. New York: American Institute of Physics, 1994.

[2] D. B. Kilfoyle and A. B. Baggeroer, "The state of the art in underwater acoustic telemetry," *Oceanic Engineering, IEEE Journal of,* vol. 25, pp. 4-27, 2000.

[3] T. C. Yang, "Properties of underwater acoustic communication channels in shallow water," *J Acoust Soc Am,* vol. 131, pp. 129-45, Jan 2012.

[4] P. Bello, "Measurement of random time-variant linear channels," *Information Theory, IEEE Transactions on,* vol. 15, pp. 469-475, 1969.

[5] L. Weichang and J. C. Preisig, "Estimation of Rapidly Time-Varying Sparse Channels," *Oceanic Engineering, IEEE Journal of,* vol. 32, pp. 927-939, 2007.

[6] J. C. Preisig and G. B. Deane, "Surface wave focusing and acoustic communications in the surf zone," *J Acoust Soc Am,* vol. 116, p. 2067, 2004.

[7] S. H. Byun, S. M. Kim, S. G. Kim, and Y. K. Lim, "Estimation of Transmission Loss and Channel Parameters of Shallow Underwater Acoustic Communication Channel," in *Proceedings of the Acoustical Society of Korea Conference (in Korean)*, Jeju, 2008, pp. 83-88.

[8] B. H. Fleury, M. Tschudin, R. Heddergott, D. Dahlhaus, and K. Ingeman Pedersen, "Channel parameter estimation in mobile radio environments using the SAGE algorithm," *Selected Areas in Communications, IEEE Journal on,* vol. 17, pp. 434-450, 1999.

[9] M. H. E. Tschudin, "Analyse und Vergleich von hochauflosenden Verfahren zur Funkkanalparameterschatzung," Eidgenossische Technische Hochschule, Zurich, 1999.

[10] S. H. Byun, S. M. Kim, Y. K. Lim, and W. Seong, "Measurement of angular power profile at an array receiver in a shallow underwater acoustic channel," *J Acoust Soc Am,* vol. 123, pp. 3903-3903, 2008.

[11] M. Feder and E. Weinstein, "Parameter estimation of superimposed signals using the EM algorithm," *Acoustics, Speech and Signal Processing, IEEE Transactions on,* vol. 36, pp. 477-489, 1988.

[12] S. M. Kay, *Fundamentals of statistical signal processing : estimation theory*. Englewood Cliffs, N.J.: PTR Prentice-Hall, 1993.

[13] A. P. Dempster, N. M. Laird, and D. B. Rubin, "Maximum likelihood from incomplete data via the EM algorithm," *Journal of the Royal Statistical Society. Series B (Methodological),* pp. 1-38, 1977.

[14] J. A. Fessler and A. O. Hero, "Space-alternating generalized expectation-maximization algorithm," *Signal Processing, IEEE Transactions on,* vol. 42, pp. 2664-2677, 1994.

[15] S. G. Mallat and Z. Zhang, "Matching pursuits with time-frequency dictionaries," *Signal Processing, IEEE Transactions on,* vol. 41, pp. 3397-3415, 1993.

[16] Y. C. Pati, R. Rezaiifar, and P. Krishnaprasad, "Orthogonal matching pursuit: Recursive function approximation with applications to wavelet decomposition," 1993, pp. 40-44 vol. 1.

[17] S. F. Cotter and B. D. Rao, "Sparse channel estimation via matching pursuit with application to equalization," *Communications, IEEE Transactions on,* vol. 50, pp. 374-377, 2002.

[18] C. Carbonelli and U. Mitra, "A Simple Sparse Channel Estimator for Underwater Acoustic Channels," in *OCEANS 2007*, 2007, pp. 1-6.

[19] C. Carbonelli, S. Vedantam, and U. Mitra, "Sparse Channel Estimation with Zero Tap Detection," *Wireless Communications, IEEE Transactions on,* vol. 6, pp. 1743-1763, 2007.

[20] T. Kang and R. A. Iltis, "Iterative Carrier Frequency Offset and Channel Estimation for Underwater Acoustic OFDM Systems," *Selected Areas in Communications, IEEE Journal on,* vol. 26, pp. 1650-1661, 2008.

[21] M. Stojanovic, "OFDM for underwater acoustic communications: Adaptive synchronization and sparse channel estimation," in *Acoustics, Speech and Signal Processing, 2008. ICASSP 2008. IEEE International Conference on*, 2008, pp. 5288-5291.

[22] W. U. Bajwa, J. Haupt, G. Raz, and R. Nowak, "Compressed channel sensing," in *Information Sciences and Systems, 2008. CISS 2008. 42nd Annual Conference on*, 2008, pp. 5-10.

[23] W. U. Bajwa, J. Haupt, A. M. Sayeed, and R. Nowak, "Compressed channel sensing: A new approach to estimating sparse multipath channels," *Proceedings of the IEEE*, vol. 98, pp. 1058-1076, 2010.

[24] C. R. Berger, Z. Shengli, J. C. Preisig, and P. Willett, "Sparse Channel Estimation for Multicarrier Underwater Acoustic Communication: From Subspace Methods to Compressed Sensing," *Signal Processing, IEEE Transactions on*, vol. 58, pp. 1708-1721, 2010.

[25] S. S. Chen, D. L. Donoho, and M. A. Saunders, "Atomic decomposition by basis pursuit," *SIAM Review*, pp. 129-159, 2001.

[26] E. J. Candès, "The restricted isometry property and its implications for compressed sensing," *Comptes Rendus Mathematique*, vol. 346, pp. 589-592, 2008.

[27] D. Needell and J. A. Tropp, "CoSaMP: Iterative signal recovery from incomplete and inaccurate samples," *Applied and Computational Harmonic Analysis*, vol. 26, pp. 301-321, 2009.

[28] P. Bello, "Characterization of Randomly Time-Variant Linear Channels," *Communications Systems, IEEE Transactions on*, vol. 11, pp. 360-393, 1963.

[29] E. J. Candes, Y. C. Eldar, D. Needell, and P. Randall, "Compressed sensing with coherent and redundant dictionaries," *Applied and Computational Harmonic Analysis*, vol. 31, pp. 59-73, 2011.

[30] B. H. Fleury, "First-and second-order characterization of direction dispersion and space selectivity in the radio channel," *Information Theory, IEEE Transactions on*, vol. 46, pp. 2027-2044, 2000.

[31] J. A. Tropp and S. J. Wright, "Computational methods for sparse solution of linear inverse problems," *Proceedings of the IEEE*, vol. 98, pp. 948-958, 2010.

[32] A. V. Oppenheim, R. W. Schafer, and J. R. Buck, *Discrete-time signal processing - 2nd edition*. Upper Saddle River, NJ: Prentice hall, 1999.

[33] M. F. Duarte and R. G. Baraniuk, "Spectral compressive sensing," *preprint*, 2010.

[34] J. A. Tropp, "Greed is good: Algorithmic results for sparse approximation," *Information Theory, IEEE Transactions on*, vol. 50, pp. 2231-2242, 2004.

[35] M. Wax and T. Kailath, "Detection of signals by information theoretic criteria," *Acoustics, Speech and Signal Processing, IEEE Transactions on*, vol. 33, pp. 387-392, 1985.

[36] M. Wax, *Detection and estimation of superimposed signals*: Stanford University, 1985.

[37] L. N. Trefethen and D. Bau, *Numerical linear algebra*: Society for Industrial Mathematics, 1997.

[38] G. Davis, S. Mallat, and M. Avellaneda, "Adaptive greedy approximations," *Constructive approximation*, vol. 13, pp. 57-98, 1997.

[39] D. Tse and P. Viswanath, *Fundamentals of wireless communication*. Cambridge, UK; New York: Cambridge University Press, 2006.

[40] H. Krim and M. Viberg, "Two decades of array signal processing research: the parametric approach," *Signal Processing Magazine, IEEE*, vol. 13, pp. 67-94, 1996.

[41] D. H. Johnson and D. E. Dudgeon, *Array signal processing: concepts and techniques*: P T R Prentice Hall, 1993.

[42] L. Balogh and I. Kollar, "Angle of arrival estimation based on interferometer principle," in *Intelligent Signal Processing, 2003 IEEE International Symposium on*, 2003, pp. 219-223.

[43] C. T. Tindle, G. Deane, and J. Preisig, "Multipath reflection from surface waves," *J Acoust Soc Am*, vol. 123, p. 3086, 2008.

초 록

시변 스파스 수중 음향 통신 채널 매개변수 추정

서울대학교 대학원
조선해양공학과
변 성 훈

본 논문은 시변 스파스 수중 음향 통신 채널의 매개변수 추정 문제를 다루고 있으며, 시변 다중경로 채널 환경에서 각 다중경로 성분의 지연 시간, 입사각, 도플러 편이 그리고 복소 진폭을 정확하게 추정할 수 있는 새 기법을 제안하였다.

새로 제안된 기법은 광대역 수중 음향 통신 채널이 가지는 스파스 구조를 이용하며, 가설의 채널 매개변수로 사전 행렬을 만들고 사전의 열과 잔차 신호와의 매칭 퍼수트를 이용해 반복적으로 다중경로 성분의 매개변수를 추정한다.

고려해야 하는 매개변수 공간의 차원이 크기 때문에, 사전의 크기 또한 매우 크며, 특히 효과적으로 스파스 근사를 위해 매개변수 공간을 오버샘플링하는 경우에는 사전의 크기가 구현 불가능할 정도로 급격히 커지게 된다.

이를 방지하기 위하여, 본 연구에서는 식별 단계와 추정 단계로 구성되는 2단계 과정을 통해 매개변수 추정이 수행되도록 하였다. 먼저 첫 번째 식별 단계에서는 미리 계산된 낮은 코히어런스의 사전을 이용해 매개변수 초기값을 얻는다. 두 번째 추정 단계에서는 식별 단계에서 얻어진 초기값 근처를 오버샘플링하여 코히어런트 사전을 구성하고, 구성된 사전의 열에 잔차 신호를 투영하여 다중경로 성분의 매개변수를 추정하도록 하였다. 추정 단계에서 코히어런트 사전을 사용할 때 발생하는 메모리 및 계산 요구량을 감소시키기 위하여 전체 매개변수 공간을

더 작은 차원의 공간으로 나누고 나뉘어진 공간에 대해 선택적으로 매개변수 추정을 수행하는 space-alternating 방법을 도입하여 사전의 크기를 줄이고 반복 과정의 계산 요구량을 감소시키고자 하였다.

제안된 기법의 성능 평가를 위하여 몬테카를로 수치 시뮬레이션과 실험 자료 분석을 수행하였다.

수치 시뮬레이션에서는 두 개의 근접한 경로로 구성되는 채널 데이터를 만들고 각 경로 성분의 매개변수를 추정하는 수치 실험을 수행하였으며, 그 결과 제안된 기법이 기존의 상관 기반 방법들이 가지는 해상도 한계 값 이하의 매개변수 차이를 구분할 수 있는 분해 성능을 지니고 있음을 확인하였다.

또, 인공적으로 파도를 만들 수 있는 대형 수조 실험 자료 분석을 통해 수면에서 반사된 신호의 추정 결과와 이론적인 모델에 의한 예측 결과가 일치하는 것을 확인하였다.

마지막으로 얕은 바다에서 송신기와 수신기 사이의 거리를 변화시켜가며 획득한 채널 측정 자료를 이용해 제안된 기법의 성능을 검증하였다. 이 때 채널 측정 환경의 실제 채널 매개변수 값을 알 수 없으므로, 측정 자료로부터 얻어지는 채널 특성 함수와 추정된 매개변수를 이용해 계산된 채널 특성 함수를 비교하여 추정된 매개변수의 유효성을 검증하였다. 분석 결과, 두 방법으로 얻어진 채널 특성 함수는 서로 매우 유사하게 나타났으며, 이는 제안된 기법이 실해역 채널 추정에도 유용하게 활용될 수 있음을 보여준다.

주요어: 채널 추정, 배열 신호 처리, 매칭 퍼수트, 탐욕 알고리듬, 스파스 추정, 시변 다중경로 채널
학 번: 2006-30180

국문 초록 용어 참조 표

한글	영어
스파스	sparse
사전	dictionary
가설의	hypothesized
잔차 신호	residual signal
열	column
매칭 퍼수트	matching pursuit
탐욕 알고리듬	greedy algorithm
코히어런스	coherence
식별	identification
몬테카를로	Monte Carlo
추정	estimation
상관	correlation

감사의 글

제가 처음 박사 과정에 입학한 것이 2006년도이니까 벌써 6년이 넘는 시간이 흘렀습니다. 짧지 않은 시간이지만 제가 무사히 학위 과정을 마치고 이 논문을 제출할 수 있게 된 것은 많은 분들의 도움이 있었기 때문입니다. 부족하나마 본 논문의 지면을 빌려 감사의 뜻을 전하고자 합니다.

먼저 제 지도교수님이신 성우제 교수님께 감사를 드리고 싶습니다. 학위 과정 동안 많은 점들을 지도해주시고 배려해주셔서 여기까지 올 수 있었습니다. 뵈면 뵐수록 배울 점들이 더 많이 느껴지는 분이셨습니다. 그리고 바쁘신 중에도 제 논문의 심사를 맡아주시고 건설적인 조언을 아끼지 않은 서울대 최항순 교수님과 이근화 교수님 그리고 국방과학연구소의 김성일 박사님과 세종대학교 임준석 교수님께도 감사의 말씀을 드리고 싶습니다. 이렇게 훌륭한 심사위원들을 모시고 논문 심사를 받을 수 있었던 큰 행운을 제가 충분히 활용했는지 못내 아쉬움이 남습니다.

제가 10년 넘게 근무하며 연구원으로서의 꿈을 키워올 수 있게 해준 대전 한국해양과학기술원의 동료들과 선후배님들께도 감사의 마음을 전합니다. 제가 다시 수중음향 분야의 연구를 할 수 있도록 후원해주신 임용곤 박사님과 이판묵 박사님 그리고 만날 때마다 응원의 말씀을 아끼지 않는 우리 홍섭 부장님과 최혁진 박사님, 전태병 박사님, 성홍근 박사님께도 감사의 말씀을 드립니다. 그리고 연구실 선배이신 이종무 박사님과 박철수 박사님께도 특별한 감사의 말씀을 전합니다. 특히 학위 논문 심사 기간 동안 함께 학교를 오가며 박철수 박사님께서 해주신 조언들은 제가 안정감을 찾고 논문 연구에 집중할 수 있도록 해주었습니다.

항상 성실한 자세로 저에게 모범이 되어주신 김시문 박사님, 박종원 박사님, 김승근 박사님, 윤창호 박사님께도 감사의 말씀을 전합니다. 본 논문에 사용된 귀중한 실험 자료들은 김시문 박사님의 주도아래 여러 동료들의 도움으로 얻어진 것들임을 밝혀둡니다. 그리고 최영철 박사와 김기훈 박사, 조석규 박사, 오상우

군에게도 진심 어린 고마움을 전합니다. 여러 면에서 서투른 제게 아낌없는 조언을 통해 관련 연구 분야에 대한 시각을 넓혀 주고 연구소 생활에 활력소가 되어준 훌륭한 동료이자 친구들이었습니다.

연구실 후배들 – 추영민, 김동호, 김병욱, 현아라, 박지수, 양해상, 이정철, 조세현, 박중용, 정영철 그리고 Derek - 연구실 선배를 위해 적극 나서서 도와주고 진심으로 학위 통과를 축하해주는 후배들의 생기 발랄한 모습을 보며 제가 얼마나 재미없게 살고 있는 지 배웠습니다.

본 지면만으로는 도저히 고마움을 갚을 수 없는 분들이 있습니다. 언제나 물심양면으로 후원해주시는 아버지, 어머니, 성용이 가족 그리고 틈틈이 애들을 돌봐주며 논문을 준비할 수 있도록 배려해주신 존경하는 장인 어른, 장모님께 특별한 감사를 드리고 싶습니다.

그리고 마지막으로 사랑하는 내 가족 - 너무나도 큰 헌신을 보여준 아내 미혜와 사랑스런 자녀들, 지수, 희수 그리고 도현이 - 이들은 제 삶에 있어 기쁨의 원천입니다. 일과 논문 준비로 소홀할 수 밖에 없었던 가족들에게 미안한 마음뿐이었는데 앞으로 모두 다 갚을 수 있도록 훌륭한 남편과 아빠가 될 것을 다짐합니다.